Stem Cells, 2024, **XX**, 1–21
https://doi.org/10.1093/stmcls/sxad094
Advance access publication 6 January 2024
Original Research

Human iPSC-Based Model of COPD to Investigate Disease Mechanisms, Predict SARS-COV-2 Outcome, and Test Preventive Immunotherapy

Rania Dagher[1,‡], Aigul Moldobaeva[1,‡], Elise Gubbins[1], Sydney Clark[1], Mia Madel Alfajaro[2,3], Craig B. Wilen[2,3], Finn Hawkins[4,5], Xiaotao Qu[6], Chia Chien Chiang[6], Yang Li[1], Lori Clarke[7], Yasuhiro Ikeda[7], Charles Brown[8], Roland Kolbeck[9], Qin Ma[10], Mauricio Rojas[11], Jonathan L. Koff[12,#], Mahboobe Ghaedi[*,1,#]

[1]Bioscience COPD/IPF, Research, and Early Development, Respiratory & Immunology, BioPharmaceuticals R&D, AstraZeneca, Gaithersburg, MD, USA
[2]Department of Laboratory Medicine, Yale School of Medicine, New Haven, CT, USA
[3]Department of Immunobiology, Yale School of Medicine, New Haven, CT, USA
[4]Center for Regenerative Medicine of Boston University and Boston Medical Center, Boston, MA, USA
[5]The Pulmonary Center and Department of Medicine, Boston University, School of Medicine, Boston, MA, USA
[6]Data Science and Artificial Intelligence, BioPharmaceuticals R&D, AstraZeneca, Gaithersburg, MD, USA
[7]Cell Therapeutics, Antibody Discovery, and Protein Engineering, BioPharmaceuticals R&D AstraZeneca, Gaithersburg, MD, USA
[8]CPSS, BioPharmaceuticals R&D AstraZeneca, Gaithersburg, MD, USA
[9]Spirovant Sciences, Philadelphia, PA, USA
[10]Department of Biomedical Informatics, College of Medicine, Ohio State University, Columbus, OH, USA
[11]Department of Internal Medicine, Division of Pulmonary, Critical Care & Sleep Medicine, Davis Heart & Lung Research Institute, Ohio State University, Columbus, OH, USA
[12]Department of Medicine, Section of Pulmonary, Critical Care & Sleep Medicine, Yale School of Medicine, New Haven, CT, USA

[*]Corresponding author: Mahboobe Ghaedi, Bioscience COPD/IPF, Research and Early Development, Respiratory & Immunology, BioPharmaceuticals R&D, AstraZeneca, Gaithersburg, MD 20878, USA. Email: mahboobe.ghaedi@astrazeneca.com
[‡]Equal contribution (shared first authorship).
[#]Equal contribution (shared last authorship).

Abstract

Chronic inflammation and dysregulated repair mechanisms after epithelial damage have been implicated in Chronic obstructive pulmonary disease (COPD). However, the lack of ex vivo-models that accurately reflect multicellular lung tissue hinders our understanding of epithelial-mesenchymal interactions in COPD. Through a combination of transcriptomic and proteomic approaches applied to a sophisticated in vitro iPSC-alveolosphere with fibroblasts model, epithelial-mesenchymal crosstalk was explored in COPD and following SARS-CoV-2 infection. These experiments profiled dynamic changes at single-cell level of the SARS-CoV-2-infected alveolar niche that unveiled the complexity of aberrant inflammatory responses, mitochondrial dysfunction, and cell death in COPD, which provides deeper insights into the accentuated tissue damage/inflammation/remodeling observed in patients with SARS-CoV-2 infection. Importantly, this 3D system allowed for the evaluation of ACE2-neutralizing antibodies and confirmed the potency of this therapy to prevent SARS-CoV-2 infection in the alveolar niche. Thus, iPSC-alveolosphere cultured with fibroblasts provides a promising model to investigate disease-specific mechanisms and to develop novel therapeutics.

Key words: COPD; emphysema; disease modeling; induced pluripotent stem cells (iPSC); alveolospheres; type 2 alveolar epithelial cells; mesenchyme crosstalk; SARS-CoV-2; drug testing; therapeutic monoclonal antibodies.

Received: 24 April 2023; Accepted: 22 August 2023.

Graphical Abstract

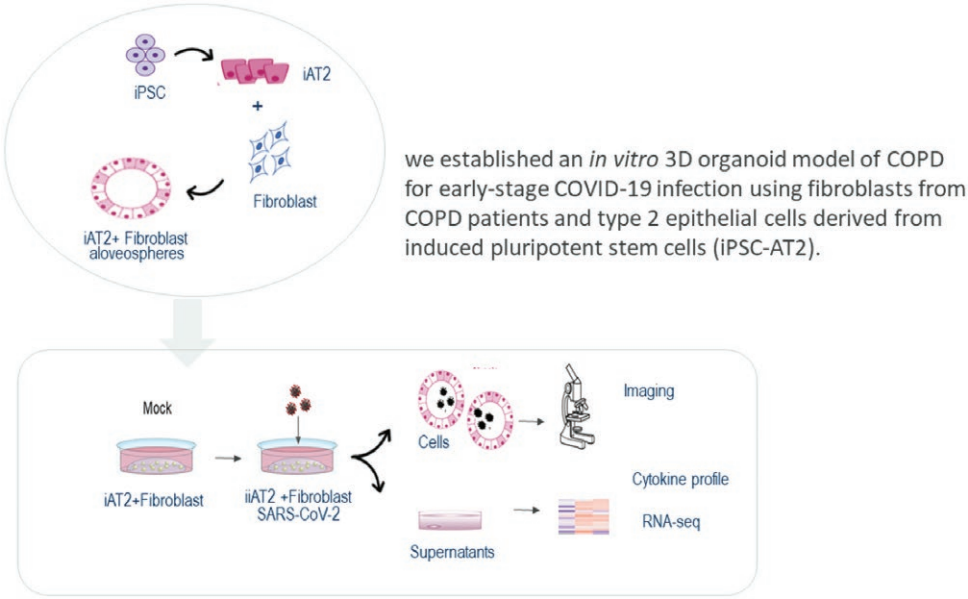

Introduction

Chronic obstructive pulmonary disease (COPD) is characterized by airflow obstruction, structural lung defects, and chronic respiratory symptoms.[1] In susceptible individuals, smoking or other environmental exposures induce inflammation and injury of the airways and alveoli that leads to pathological changes that include: (1) small airway remodeling associated with bronchitis and/or bronchiolitis, and (2) destruction of the alveolar-capillary unit that is associated with emphysema.[1-3] In COPD, autoimmunity, aging, exaggerated apoptosis, and inadequate repair mechanisms[4] have been implicated in alveolar destruction and endothelial injury. In addition, recurrent environmental insults result in acute and chronic inflammation that is mediated by imbalances in proteases, antiproteases, and oxidative stress. The result is extracellular matrix degradation and alveolar destruction.[5] Chronic inflammation and dysregulated lung repair after epithelial injury may contribute to distinct clinical entities of emphysema, which continues to be a limitation in our understanding of the cellular composition and dynamics of the COPD alveolar-capillary unit.[6]

A major roadblock in studying the alveolar niche in COPD is the lack of ex vivo models that accurately reflect multicellular lung tissue. Access to tissue from patients with COPD is limited, and almost universally reflects end-stage disease because this tissue is obtained from individuals at the time of lung transplantation or death.[7] Mouse models are inadequate because they do not reflect specific characteristics of human COPD lung disease.[8-11] This has resulted in a failure to translate efficacy and toxicity data in clinical trials from animals to humans.[12]

Induced pluripotent stem cells (iPSC) provide a powerful platform to develop disease-specific, and patient-specific in vitro models of emphysema.[13-17] Lung epithelial cells are generated from iPSCs by recapitulation of key embryonic development stages in vitro.[13-17] iPSCs allow for: (1) cellular expansion, which provides a source of replicates to study respiratory disease mechanisms,[13,18] (2) "personalized medicine" because iPSCs maintain individual human genetics, and (3) overcome challenges of obtaining donor tissue from patients, which was highlighted a particular concern during a pandemic.[19-21] Finally, iPSCs can be cultured in a self-organizing organoid culture system (eg, alveolosphere) relevant to diseases of interest. This has dramatically improved our understanding of tissue homeostasis and pathological alterations in lung disease.[13,14,16] While alveolospheres have been used to screen for factors that regulate stem cells and recapitulate lung diseases in vitro,[13,14,22] most studies have only focused on the deleterious effects of smoke and pollutant exposures to type 2 alveolar epithelial cells (AT2).[23] However, alveolospheres alone are an oversimplified model, with limited cellular and functional representation of the native alveolus, if the supporting mesenchyme is not included. For example, fibroblasts have been shown to significantly contribute to alveolar lung injury and repair responses.[6,24-26] Specifically, fibroblasts respond by producing inflammatory mediators and extracellular matrix to maintain alveolar structure after injury.[6,24] Thus, alterations in alveolar and fibroblast interactions may lead to inadequate tissue structure repair and maintenance in COPD, which needs further characterization.[6,24,27] This is highlighted by the recognition that COPD is associated with an increased risk of severe SARS-CoV-2 infection and substantial mortality rates in the COVID-19 pandemic.[28-30] Therefore, a more detailed understanding of the susceptibility of patients with COPD to SARS-CoV-2 infection, which includes identifying the cell types and pathways that are permissive to viral infection and replication, will provide novel insights into the transmissibility and pathogenesis of SARS-CoV-2 infection.[3,31]

Imbalance of AT2 death and proliferation in patients with emphysema contributes to alveolar wall destruction and impaired gas exchange. In this study, a model of iPSC-derived AT2 alveolospheres (iAT2s) with healthy and COPD fibroblasts was used to model human alveoli, and to explore factors regulating AT2 function in COPD. Using a combination of transcriptomic and proteomic approaches, these experiments provide a robust, novel characterization of fibroblast-epithelial interactions in COPD. Subsequently, SARS-CoV-2 infection was studied in this model to

characterize virus-induced host gene expression responses to infection in the alveolar compartment in a more physiologically relevant system. In addition, this model was used to investigate novel anti-SARS-CoV-2 monoclonal antibodies that inhibit the interaction of spike protein with the SARS-CoV-2 receptor, ACE2. Thus, iPSC-derived AT2 alveolospheres cultured with fibroblasts provide a novel, highly functional model to investigate pulmonary disease-specific molecular mechanisms, stimuli, and potentially novel therapeutics.

Results

Generation of iPSC-Based Alveolospheres

The iPSC line utilized in this study was provided by Dr. Darrell N. Kotton, Center for Regenerative Medicine, Boston University. Using gene-editing fluorochrome reporter constructs (GFP and tdTomato) targeted to the endogenous NKX2-1 and SFTPC loci, respectively, of BU3 NGST iPSC line (BU3 NKX2-1GFP; SFTPCtdTomato).[15] iPSC-based AT2 alveolospheres (iAT2) were generated from BU3 NGST iPSC line by following a recently reported protocol.[15,16] First, definitive endoderm (DE) was derived with STEMdiff kit induction with over 85% efficiency (Fig. 1A–1C). At day 15 of differentiation, NKX2-1$^+$ lung epithelial progenitor cells were derived at varying efficiencies from iPSC line after being exposed to a growth factor cocktail containing CHIR99021, rhBMP4, and retinoic acid (Fig. 1D–1E). iAT2 alveolospheres from an NKX2-1$^+$ progenitor population were generated from sorted GFP$^+$ NKX2-1 cells, which were replated and cultured in a growth factor cocktail in Matrigel for 2 weeks.[15] NKX2.1 cells proliferated and formed epithelial spheres that maintained variable levels of NKX2-1 (green-labeled) and SPC (red-labeled) expression (Fig. 1F–1I). Single-cell profiling at day 35 showed iAT2 alveolospheres composed of a high percentage of iAT2 SPC expressing epithelial cells with a transcriptional profile similar to human AT2[15] where an enriched expression of SFTPC, PGC, CPM, RNASE1, NAPSA, SCGB3A1, LPCAT1, and CTGF in clusters 1 and 2 was found (Fig. 1J). Electron micrograph of iAT2s published by Kotton's lab showed the presence of lamellar body in these cells.[15] In humans, lung alveoli are maintained by intermittent activation of rare "bifunctional" AT2 cells that retain surfactant biosynthesis function and also serve as stem cells that generate new AT1 cells and self-renew throughout adult life.[32-34] Here, iAT2 proliferating cells in cluster 2, which behave similarly to AT2 stem cells, were defined by the expression of MKI67 (Fig. 1J–1K). We also identified small percentages of stromal cells characterized by decreasing gradients of NAPSA and SFTPC expression with increasing gradients of VIM, IGFL2, TUBA1A, KRT17, KRT19, and HES4 (Fig. 1J–1K). These cells are in transition from epithelial to mesenchyme, which may result from the stress of dissociation and in vitro culture conditions.

Establishing an iPSC-Based Disease Model That Recapitulates Emphysema

Recently, it has been shown that AT2 cells are in specific niches that include their immediate epithelial neighbors, as well as underlying smooth muscle, fibroblasts, blood vessels, and nerves.[27,35] These niches are highly dynamic and involve cytokines, and other signaling factors, that are derived from multiple cell populations.[27,35] To explore factors regulating AT2 function specific to COPD, iAT2 cells were cultured with COPD (n = 3) and healthy (n = 3) fibroblasts isolated from human lungs in alveolospheres (Fig. 2A) to mimic the AT2-fibroblast niche in lung.[25,26] After 2 weeks, these cultures develop into an iAT2 epithelium surrounded by fibroblasts (Fig. 2A–2E). The presence of mesenchyme and organized alveolar structures is a strength of this system that provides a physiologically relevant in vitro model to study mesenchymal-epithelial crosstalk in the alveolar microenvironment in health and disease.[13,14,26] Furthermore, this 3D model grown in matrigel incorporates AT2-fibroblast mechanical cues that influence epithelial cell development in health and disease,[36] which improves this model's ability to recapitulate the human mesenchymal-epithelial niche.

In a healthy lung, the mesenchyme supports epithelial cell growth.[25,26,37] Thus, we hypothesized that iAT2 cultured with healthy fibroblast in alveolospheres (iAT2 + HFib) would receive similar support from niche. iAT2 + HFib formed more alveolospheres (Fig. 2B, 2C, 2F) compared to iAT2 cocultured with COPD fibroblasts (iAT2 + CFib); (Fig. 2D–2F), while iAT2 + CFib resulted in lower numbers of SPC expressing iAT2 in COPD alveolospheres (Fig. 2C, 2E, 2F). In addition, single-cell RNA sequencing (sc-RNA seq) profiling of iAT2 + HFib compared to iAT2 + CFib confirmed the differences in iAT2 cells in COPD and healthy alveolospheres (Fig. 2G). Of significance, the number of SPC expressing iAT2 and proliferating iAT2 cells is significantly decreased in iAT2 + CFib compared to iAT2 + HFib alveolospheres (Fig. 2G, 2H). Coculture with COPD fibroblasts impacted iAT2 cell transcripts of SFTPC, SFTPA, and induced expression of profibrotic markers, such as COL1A1, TGFB3, COL6A2, POSTN, FOSL2, and CXCL2 (Fig. 2I). Pathway analysis of sc-RNA seq data revealed that iAT2 + CFib are enriched for biological processes involved in cell aging and inflammation (Fig. 2J). Specifically, "cell death," "fibrosis," "oxidative stress," "mitochondrial dysfunction," "extracellular matrix organization," and "autophagy" pathways were significantly altered in iAT2 + CFib compared to iAT2 + HFib alveolospheres (Fig. 2I–2J). These results highlight the specificity of paracrine signaling from COPD fibroblasts to activate molecular changes and cellular responses, which favors cell aging and senescence, inflammation, fibrosis, and apoptosis in iAT2 cell cocultures. These observations corroborate with recent studies highlighting the contribution of cellular senescence and accelerated aging in COPD pathology.[38]

To verify whether our model phenocopies main features of AT2 in COPD alveolar niche, we cross-validate the transcriptomic profiles of our COPD aloveosphere with COPD lung tissues characterized by single-cell RNAseq from publicly available data.[39] By comparing the expression patterns of AT2 clusters, we found that 67.7% of our iAT2 (Clusters 1, 2) DEGs overlapped with human AT2 from COPD lung, and their corresponding pathway analyses covered the main pathological mechanisms enriched in COPD AT2, particularly, cellular senescence, apoptosis, oxidative stress, and epithelial-mesenchhyme transition (Fig. 2K).

In response to lung injury, fibroblasts, part of lung mesenchyme, undergo transient phenotypical changes to promote tissue repair through secretion of repair-associated factors and extracellular matrix (ECM).[32]; However, COPD is characterized by an impaired fibroblast response to chronic epithelial injury where diseased fibroblasts exhibit impaired proliferation and migration. Therefore, to understand the effects of lung fibroblasts on AT2 cells, sc-RNA seq was used

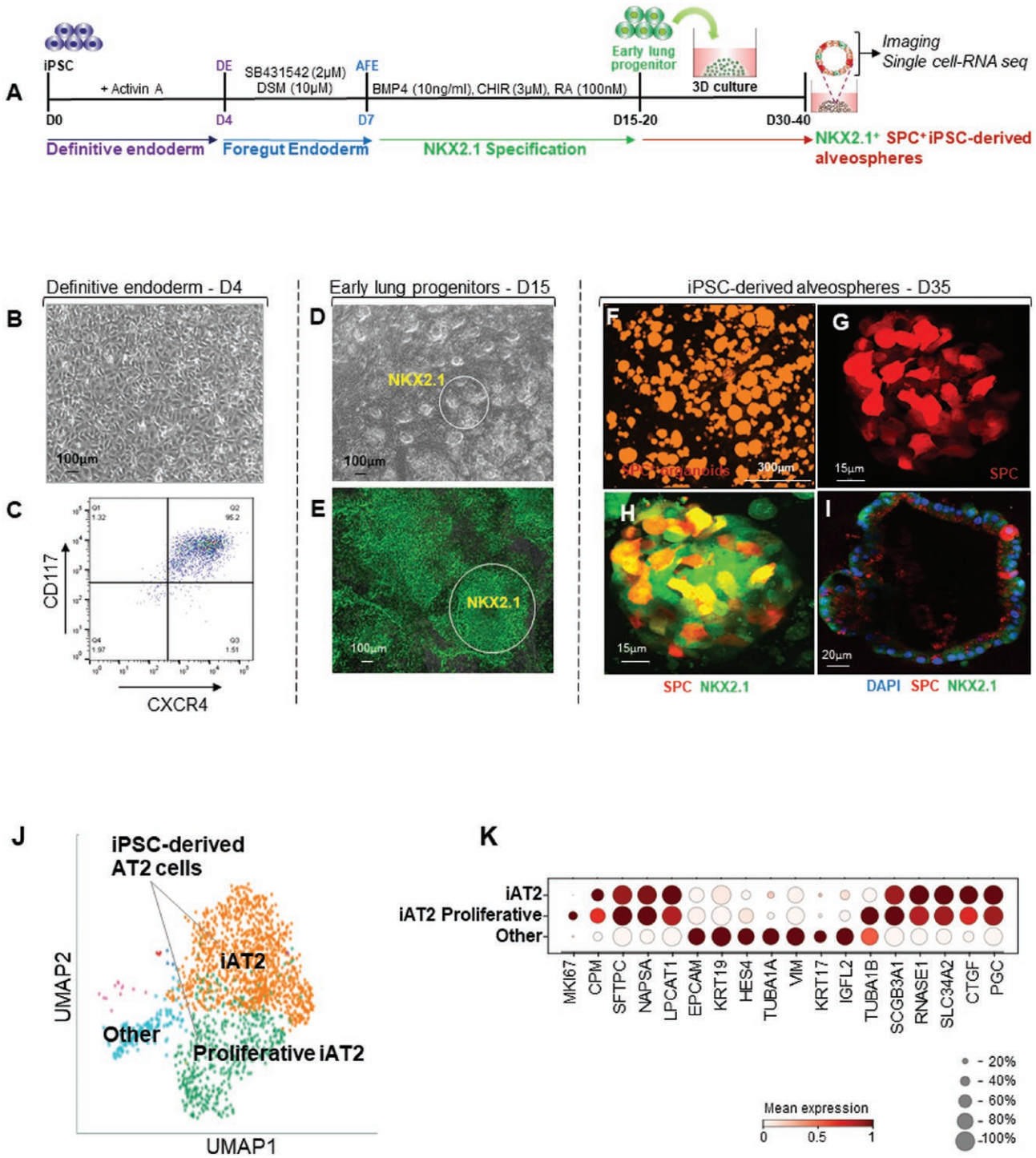

Figure 1. Differentiation of human induced pluripotent cells (hiPSC) to lung progenitors and alveolar epithelial type 2 (iAT2). (**A**) Schematic of directed differentiation protocol from human iPSCs to NKX2-1$^+$ endodermal lung progenitors and type 2 alveolar epithelium. (**B**, **C**) Representative phase-contrast images of definitive endoderm (Scale bar = 100 μm) and day 4 FACS plot showing CD117 and CXCR4 expression in DE. (**D**, **E**) Phase-contrast and immunofluorescence image of day 15 NKX2-1$^+$ cells. Scale bars = 100. (**F-H**) Representative images of SPC$^+$ alveolospheres and SPC$^+$/NKX2.1$^+$ alveolospheres. Scale bars are 300 μm and 15 μm, respectively. (**I**) Representative immunofluorescent image of SPC and NKX2.1 in cross-section of iAT2 alveolospheres at day 35. Scale bars = 20 μm. (**J**) t-SNE plot of single-cell-RNA seq of alveolar epithelial cells derived from iPSC at day 35. (**K**) Dot plot of cell type-specific marker gene for iAT2. Color gradient and dot size indicate for each cluster the mean marker expression and the percentage of cells expressing the marker, respectively.

to characterize lung fibroblast subtypes in iAT2 alveolospheres cocultured with COPD and healthy fibroblast cells (Fig. 3A). Transcriptomic profiling allowed the discrimination of 5 different clusters of fibroblasts (Fig. 3B). We have identified 2 prominent fibroblast subsets, Clusters 3 and 7 (51% and 21%, respectively), and to a lesser extent Cluster 0 (12%), which predominate in healthy samples. These clusters are enriched with trophic mediators such as FGF7, HGF, AREG, and TGFβI. (Fig. 3A, 3C), which suggests that these trophic fibroblasts may support iAT2 growth to promote epithelial

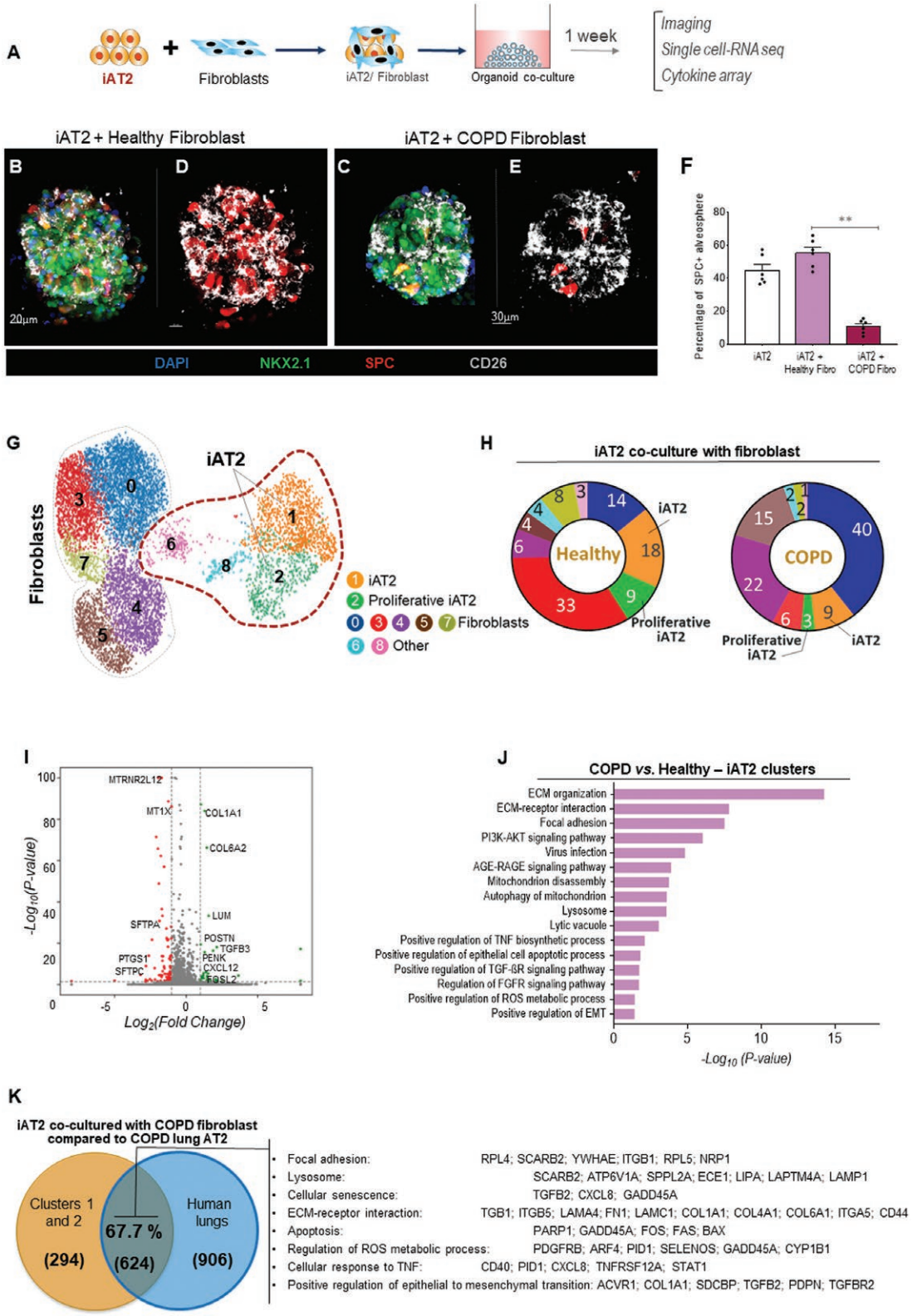

Figure 2. Coculture of iAT2 with fibroblast isolated from healthy and COPD lung in aloveosphere culture system. (**A**) Schematic of iAT2 and fibroblasts coculture system. (**B-E**) Coculture of iAT2 with healthy and COPD fibroblast. immunofluorescence stains of CD26 (fibroblast marker) and DAPI for nuclei. GFP reporter shows NKX2.1 and the red reporter shows SPC expression. Scale bars are 20 and 30 μm, respectively. (**F**) Percentages of SPC$^+$ alveolospheres in iAT2 co-coculture with healthy fibroblasts compared to iAT2 co-coculture with COPD fibroblasts. Bars represent mean ± SEM, $n = 3$. (**G**) t-SNE plot of single-cell-RNA seq of alveolar epithelial cells derived from iPSC coculture with healthy or COPD fibroblasts. (**H**) Pie chart depicting the percentage of iAT2 and fibroblast clusters in iAT2/COPD fibroblasts alveolospheres vs iAT2/healthy fibroblasts alveolospheres. (**I**) Volcano plots highlighting the most differentially expressed genes between iAT2 cocultured with COPD fibroblasts vs iAT2 cocultured with healthy fibroblasts. (**J**) Pathway analysis of biological processes in iAT2 most significantly affected by COPD and healthy fibroblasts. (*P*-value < .01). (**K**) Overlaps between differentially expressed genes (DEGs) identified from iAT2 cocultured with COPD fibroblast compared to that predicted from AT2 in human COPD lung data. Representative pathways enriched by the top-ranked overlapped DEGs were highlighted on the right of the Venn diagram.

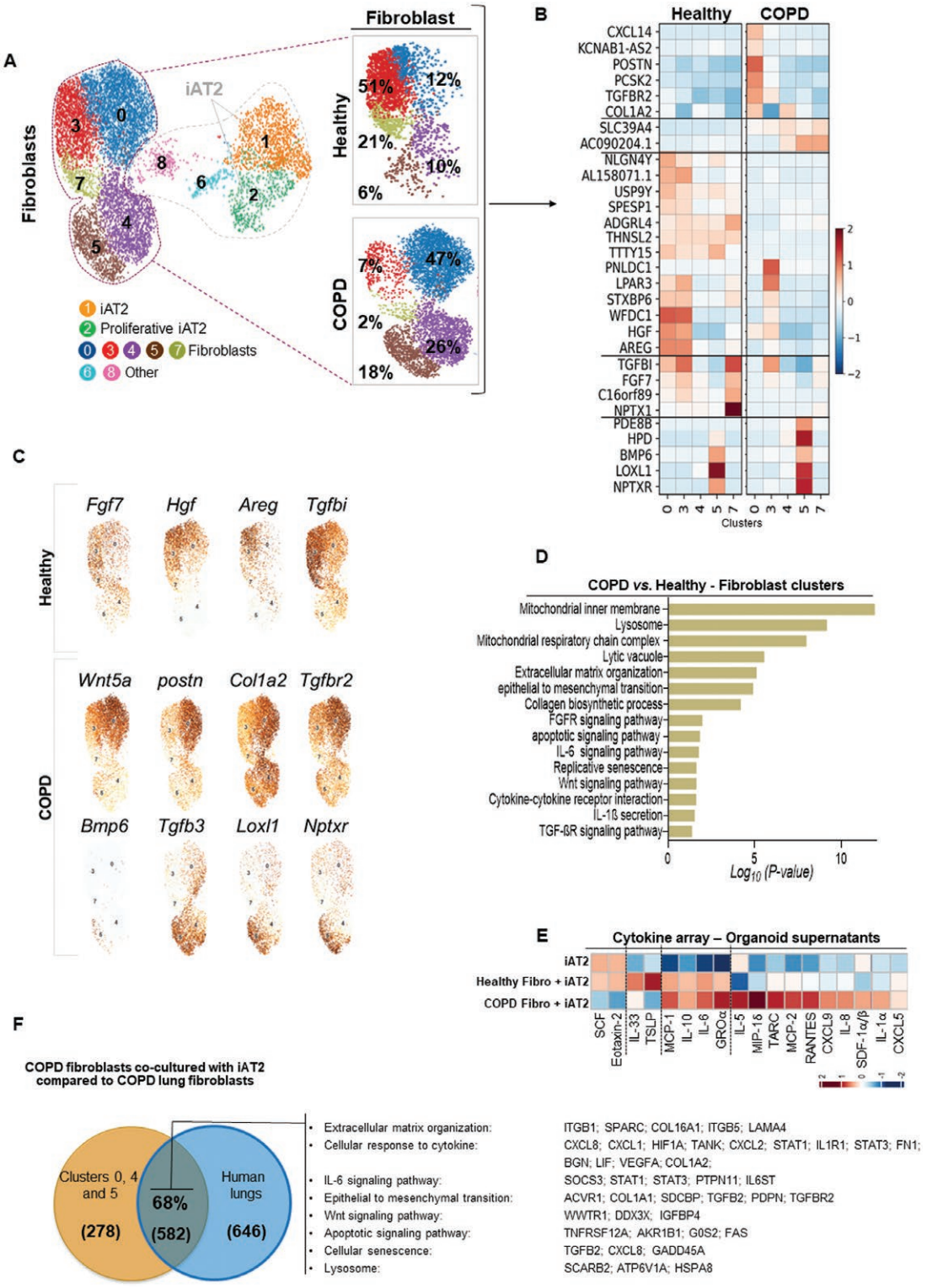

Figure 3. Sc-RNA seq of coculture of iAT2 with fibroblast isolated from healthy and COPD lung in 3D organoid system. (**A**) t-SNE plot of single-cell RNA seq of alveolar epithelial cells derived from iPSC in coculture with healthy or COPD fibroblasts. (**B**) Heatmap of differentially expressed genes (DEGs) in different clusters of COPD and healthy fibroblasts. (**C**) t-SNE plots highlight the main trophic factors expressed in healthy fibroblasts and fibrotic drivers of COPD pathology expressed in COPD fibroblasts. (**D**) Pathways and the molecular functions most significantly activated in healthy and COPD lung fibroblasts in a coculture system. (**E**) Heat map of cytokines and chemokines secreted from iAT2, iAT2/healthy fibroblast alveolospheres, and iAT2/COPD fibroblasts alveolospheres. (**F**) Overlaps between DEGs identified from COPD fibroblasts cocultured with iAT2 compared to that predicted from fibroblasts in human COPD lung data. Representative pathways enriched by the top-ranked overlapped DEGs were highlighted on the right of the Venn diagram.

regeneration in the alveolar niche. In line with this observation, lung trophic fibroblasts were reported to lie near individual AT2 cells; these fibroblasts secrete homeostatic levels of repair-associated factors such as Wnt and FGF that are required for activation of a subpopulation of AT2 cells, with stem cell activity, to promote alveolar regeneration.[26,35,40]

Transcriptomic profiling of COPD fibroblasts showed enrichment of pro-fibrotic markers, such as Wnt5a, TGFβ, LOXL1, POSTN, CXCL14, COLIA2, and NPTXR in Clusters 0, 4, and 5 (Fig. 3A–3C), while the expression of the trophic factors, such as FGF7, HGF, AREG, were downregulated. Consistent with prior observations in COPD fibroblast,[24] our findings highlight the contribution of these pro-fibrotic clusters in the COPD alveolar niche by promoting paracrine signals involved in inflammation (CXCL14, LOXL1), fibrosis (COLIA1, TGFBR2), and apoptosis in iAT2 (Fig. 3B–3C), which may have an association with "accelerated aging."[38,41,42] To determine the molecular pathways involved in the "accelerated aging" in an alveolar niche, pathway analyses were compared between COPD and healthy fibroblasts in iAT2 aloveosphere cocultures (Fig. 3D). The pathway analysis showed changes in "cell proliferation and differentiation," "mitochondrial function," "extracellular matrix organization," "epithelial-mesenchymal transition," "apoptosis," "senescence," and "inflammation" in COPD fibroblasts. In addition, Wnt, TGFβ, IL6, IL1β, and FGFR signaling were the top enriched pathways in COPD fibroblasts (Fig. 3D). Thus, these in vitro findings significantly improve upon prior observations,[12,15,36] and suggest that developing human iAT2 epithelia depends on fibroblast-AT2 crosstalk in the alveoli microenvironment. In addition, these effects are influenced by signals involving canonical Wnt, AREG, EGF, and FGF, secreted factors or extracellular vesicles, and endogenous and exogenous stimuli of lung inflammation.

Next, we compared transcriptomes profiles of COPD fibroblasts in our aloveosphere coculture system with human fibroblasts from COPD lung,[39] and confirmed significant overlap (68% of our DEGs) between the 2 datasets. Although human fibroblasts from COPD lungs show a higher number of DEGs compared to our in vitro system due potentially to changes in matrix stiffness, the main pathological hallmarks of COPD fibroblasts were conserved, as evidenced by the enrichment in pathological pathways involved in cell senescence, ECM deposition, and pro-inflammatory cytokines (ie, IL6, CXCL8, CXCL1, and others), and altered WNT signaling (Fig. 3F).

In COPD, lung inflammation persists even after smoking cessation[43] because of cellular stress pathways and telomere shortening, which leads to cellular senescence, increased cytokine production, and cell cycle arrest in lung cells.[38,44] Senescence is a cell-autonomous process that results in profound effects on neighboring cells via the action of senescence-associated secretory phenotype (SASP) mediators.[41,42,44] Because multiple cell senescence pathways were found enriched in COPD fibroblasts cocultured with iAT2 alveolospheres, the secreted cytokines in cell culture supernatants from organoid cocultures were measured (Fig. 3E). Cytokine and chemokine protein array revealed distinctive functional properties related to host defense and innate immune responses (Fig. 3E). Compared to iAT2 alone, iAT2 + HFib produced increased amounts of IL-33 and TSLP, alarmins that are involved in lung innate immunity in response to epithelial injury.[45-47] By contrast, iAT2 + CFib alveolospheres significantly decreased alarmin production and showed increased involvement of innate and adaptive immunity, such as: monocyte/macrophage recruitment (ie, MCP1/CCL2 and MCP2/CCL8),[48] lymphocyte infiltration (ie, CXCL9/MIG), neutrophil chemotaxis (CXCL8/IL-8, IL-6), Th2-inflammation (ie, IL-5, CCL17/TARC, and RANTES), which have all been implicated in COPD pathogenesis (Fig. 3E). Taken together, these findings suggest that COPD organoid cocultures exhibit a compromised "inflammatory status" that may lead to extensive lung damage and facilitate recurrent infection(s).[49]

In Vitro Modeling of Epithelial-Fibroblast Interactions at Air-Liquid Interface

To better investigate epithelial-fibroblast interactions, and to monitor phenotypic changes in iAT2 function when exposed to air, iAT2 cells were cultured in air-liquid interface (ALI) (Fig. 4A). At ALI, iAT2 cultures generated epithelial monolayers of pure iAT2s with apical-basal polarization and barrier integrity. These cultures showed increased expression of SPC without AQP-5, as assessed by confocal microscopy (Fig. 4C). Gene expression profiling of 2D-ALI iAT2 cultures confirmed the expression of other AT2-specific markers SFTPB, SFTPC, SFTPD, SFTPA1, SFTPA2, NAPSA, PGC as well as AT1-specific markers HOPX and AGER (Fig 4B). Taken together, these results suggest that ALI iAT2 cell cultures mimic human AT2 characteristics. Importantly, this technique allows for in vitro experimental conditions for future mechanistic studies of inflammation, injury (eg, mechanical stretch), or inhaled toxins (eg, cigarette smoke).

Because lung epithelial-microenvironment interactions contribute to cell functions via cytokines and other factors, we sought to examine the impact of paracrine factors from COPD and healthy fibroblasts on functionality of iAT2 cells in ALI cultures (Fig. 4D–4E, 4F–4G). Because AT2 cell apoptosis has been previously reported in the lung of emphysematous subjects as a potential contributor to the loss of alveoli,[50] we measured SPC surface volume in iAT2-fibroblast cocultures and observed a significant reduction of SPC surface volume in iAT2 cells cultured with COPD fibroblasts compared to iAT2 cells cultured with healthy fibroblasts after 3 and 7 days (Fig. 4H). This confirms the potential for paracrine factors secreted by COPD fibroblasts to induce cell apoptosis or epithelial-mesenchymal transition in iAT2 as evidenced by the decreased expression of SPC while GFP-NKX2.1 expression remained unchanged (Fig. 4F–4G). Next, cytokines and chemokines secreted by iAT2 cells and COPD and healthy fibroblasts were analyzed in the supernatants of ALI cocultures. Interestingly, levels of IL-33 and TSLP seem to be further depleted in iAT2 cultures with COPD fibroblasts compared to iAT2 cell cultures with healthy fibroblasts, or iAT2 cell cultures alone. Consistent with our previous data in iAT2/fibroblast alveolospheres, iAT2 cocultures with healthy fibroblasts induced the production of anti-inflammatory IL-10, as well as other cytokines involved in innate immunity (eg, MIP-1δ and MCP-1), which were also expressed in iAT2 cocultures with COPD fibroblasts (Fig. 4I).

Protein concentrations of IL-1α, IL-6, IL-8, CXCL5/ENA-78, and TNFα were higher in cell culture supernatants of iAT2 ALI cultures with COPD fibroblasts compared to iAT2 ALI cultures with fibroblasts from healthy donors (Fig. 4I). In COPD, these molecules are considered SASP mediators and are factors associated with neutrophil recruitment and inflammation.[42,45] IL-1α released from damaged epithelial cells

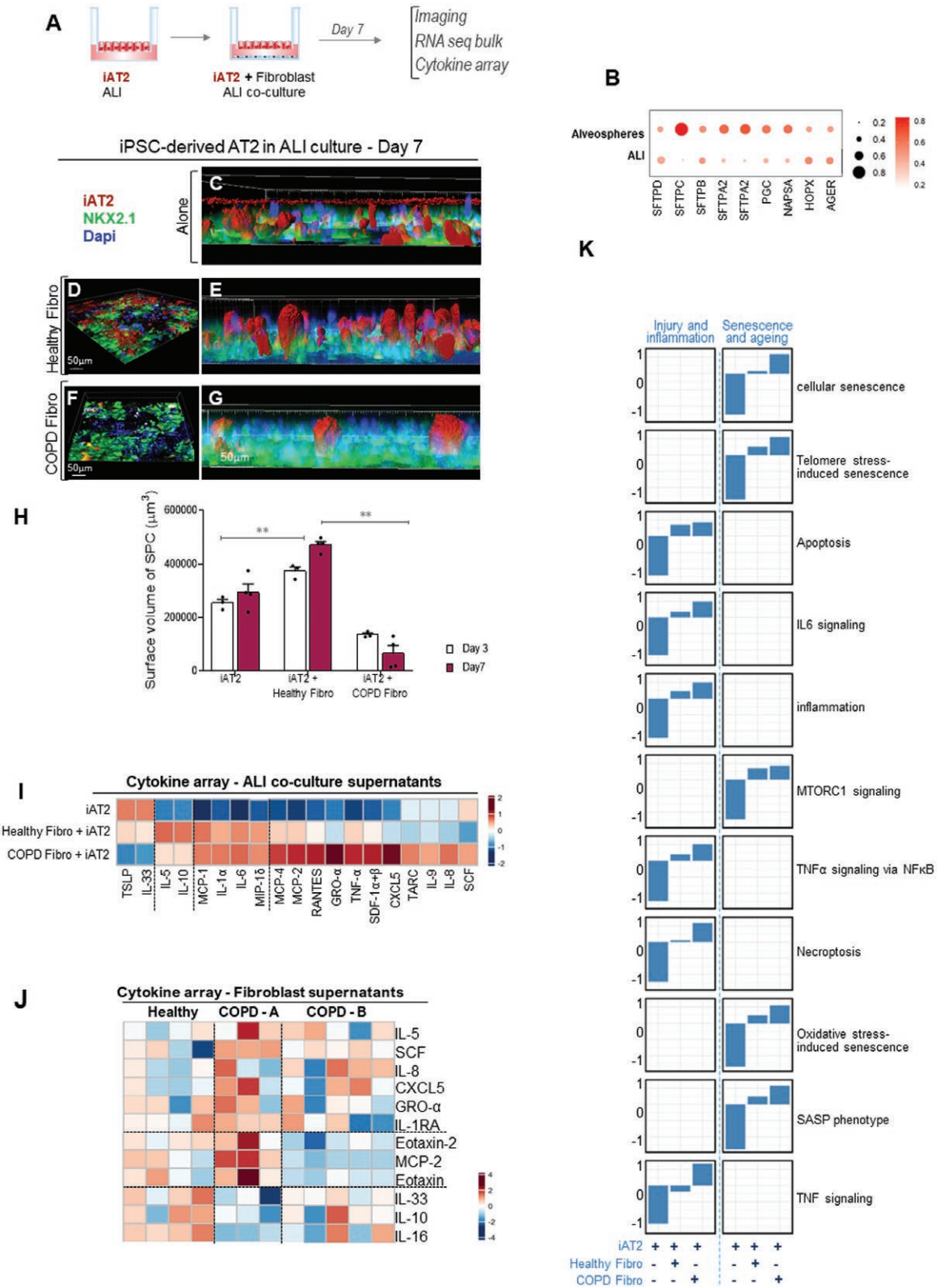

Figure 4. Coculture of iAT2 with fibroblast isolated from healthy and COPD lung in ALI culture system. (**A**) Schematic of iAT2 and fibroblasts coculture system. (**B**) Gene expression profile of iAT2 cultured in an air-liquid interface (ALI). (**C**) culture of iAT2 in 2D ALI. Red is SPC reporter, green is NKX2.1 GFP reporter and blue is DAPI staining for nuclei. Scale bar = 50 μm. (**D-G**) Cross-sectional view of (D, E) iAT2 in coculture with healthy fibroblasts and (F, G) iAT2 in coculture with COPD fibroblasts in ALI culture system. (**H**) Surface volume of SPC in iAT2 and iAT2 co-coculture with healthy and COPD fibroblasts in ALI culture system at days 3 and 7. Bars represent mean ± SEM, $n = 3$ biological replicates. (**I**) Heatmap of cytokines and chemokines secreted from iAT2 and iAT2 coculture with healthy and COPD fibroblasts. (**J**) Unbiased heat map comparisons of cytokines/chemokines secreted from healthy and COPD fibroblasts measured in vitro. (**K**) Changes in pathways including injury/inflammation and senescence/aging in iAT2 coculture with COPD fibroblast compared to coculture with healthy donors identified by changes in gene expression analyzed by RNA seq followed by gene set enrichment analysis (GSEA). The mean expression of pathway members was used to plot the bar chart for the selected pathway identified by GSEA.

is essential to trigger inflammatory responses in human lung fibroblasts.[51] Increased production of MCP-2 (CCL8) and -4 (CCL13), and RANTES observed in iAT2 ALI COPD fibroblast cocultures (Fig. 4I) are chemokines associated with increased inflammatory cell lung recruitment, which is characteristic of chronic COPD lung inflammation (Fig. 4I).

To understand the paracrine effects of COPD lung fibroblasts on iAT2 cells, cytokines/chemokines of fibroblasts isolated from COPD ($n = 9$) and healthy ($n = 10$) lungs were studied. An analysis of fibroblast cell culture supernatants by cytokine/chemokine protein array showed some heterogeneity among donors, but overall the cytokine/chemokine profile seen in healthy fibroblasts was different from COPD (Fig. 4J). For example, healthy fibroblasts exhibited higher levels of IL-10, a cytokine with inflammatory and anti-inflammatory properties, IL-16, an inflammatory cytokine that is chemotactic for lymphocytes, monocytes, and eosinophils, and the host defense alarmin IL-33 (Fig. 4J). By contrast, COPD fibroblasts displayed 2 distinct pro-inflammatory patterns that we identified as "COPD-A" and "COPD-B." Both groups exhibited higher amounts of CXCL8 and CXCL1, which are neutrophil chemokines, and CXCL5 and IL5, which are involved in eosinophil recruitment, proliferation, and differentiation (Fig. 4J). In addition, group "COPD-A" displayed increased levels of MCP-2 and eotaxin/eotaxin-2 that are associated with monocyte/macrophage and eosinophil chemotaxis,[46,48] which can be observed in subgroups of COPD characterized either by severe eosinophilic or monocytic inflammation.[45] By contrast, the secretion of anti-inflammatory and host defense mediators, IL-10, IL-33, and IL-16 were found reduced in COPD fibroblasts (Fig. 4J). In support of our findings, previous studies reported the association between a decline in lung function and lower levels of IL-10 and IL-16[52] in COPD.

To elucidate the biological processes triggered by paracrine fibroblasts signaling, RNA seq analysis on iAT2 ALI cocultures with either COPD or healthy fibroblasts was completed. Pathway analysis confirmed enrichment in pathways involved in inflammation, oxidative stress, cellular senescence, and cell death in iAT2 (Fig. 4K). Specifically, these data highlight upregulation in mitochondrial dysfunction (oxidative stress and mTOR signaling) that may lead to increased inflammation, cell senescence (eg, Telomere stress, SASP, IL-6, and TNF via NFκB pathways), and cell death (apoptosis and necroptosis) in iAT2 ALI cocultures with COPD fibroblasts (Fig. 4K). Importantly, these pathways are the most common molecular pathways contributing to COPD pathogenesis,[53] where TNF, SASP mediators, and oxidative stressors were reported to trigger apoptosis in alveolar epithelial cells.[50,53]

Similar to iAT2 COPD alveolospheres, iAT2 ALI COPD fibroblast cocultures confirmed the exaggerated inflammatory responses that may contribute to the complex immune responses in chronic lung inflammation in COPD. These results support previous studies that reported the exacerbated lung environment is associated with impaired immune responses in patients with COPD that may contribute to recurrent respiratory infections.[49,52,54]

SARS-CoV-2 Infection Dynamics in iAT2 Alveolospheres and iAT2 Co-Cultures With Fibroblasts

Because of increased susceptibility and severity in patients with COPD with SARS-CoV-2 infection,[55] a detailed understanding of COPD iAT2-fibroblast interactions that may contribute to viral infection, replication, and virus-induced inflammation is critical to understanding SARS-CoV-2 infection and pathogenesis.[3,31] Chan et al previously established COPD organoids to study host-pathogen interaction in SARS-CoV-2 in upper airway.[56] iPSC-alveolospheres and iAT2 cocultures with fibroblasts provide a promising model to investigate SARS-CoV-2 infection in alveolar niche in COPD. The human host factor angiotensin-converting enzyme 2 (ACE2) is a critical receptor for SARS-CoV-2.[57] After the viral spike protein binding to ACE2, host cell surface transmembrane serine proteases [eg, TMPRSS2 and cathepsin L (CSL)] have been implicated to facilitate viral infection.[58] However, the dynamic of AT2 responses to SARS-CoV-2 infection over time remains poorly explored, especially in COPD epithelium, which is critical to improving our understanding of host defense mechanisms and viral pathogenesis.[59]

Immunostaining for localization of ACE2 in iAT2 alveolospheres was comparable with ACE2 expression in distal lung tissue (Fig. 5A–5B). Next, iAT2 alveolospheres were infected with SARS-CoV-2 [10^4 plaque-forming units (PFU)] in 100 μL of media for 1 or 24 hours (Fig. 5C). In these experiments, alveolospheres were infected in suspension to allow for viral exposure to the apical surface of cells.[60] While there were limited changes at 1-hour post-infection, 24 hours post-infection resulted in significant changes in the iAT2 alveolospheres (Fig. 5D). iAT2 cell death observed in this model is likely relevant due to similar observations seen in vivo lung autopsies of COVID-19 decedents.[61]

To elucidate biological responses of iAT2 cells in response to SARS-CoV-2 infection, RNA seq of SARS-CoV-2-infected iAT2s at 1-3 days post-infection (dpi) were compared to mock-treated iAT2 controls (Fig. 5E–5F). Transcriptomic analysis revealed differentially expressed genes (DEGs) between SARS-CoV-2 infected and mock-treated iAT2 cells: (1) in viral infection-related markers, (2) oxidative stress, and (3) cell death-related genes (Fig. 5E–5F). The loss of AT2 cells was accompanied by the emergence of pathways involved in (1) cellular responses providing direct substrates for virion production, and (2) altered metabolism that potentially contributes to viral survival in iAT2s.[62] Subsequently, on 2 dpi and 3 dpi glycolysis and response to hypoxia decreased as SARS-CoV-2 induced iAT2 epithelial apoptosis; (3) inflammatory signaling post-SARS-CoV-2 infection; and (4) epithelial cell changes in favor of mesenchyme transition (Fig. 5F). Thus, these experiments show both upregulated and downregulated pathways in response to SARS-CoV-2 infection.

Gene expression analysis of iAT2 cells revealed significant enrichment in inflammatory pathways post SARS-CoV-2 infection, which included interferon (IFN) signaling, IFN-dependent cytokines, and RIG-I-like and NF-kB-mediated signaling over the entire time course. IFNs, and IFN-associated genes (eg, IRF1, IRF7, IRF9, IFITH, IFITM1, and IFI35), which represent an early antiviral defense, and are important regulators of innate and adaptive immune responses, were found to be upregulated in iAT2s.[63,64] Also, there was evidence for increased NF-κB-dependent activation (eg, IL-6, CXCL1, CXCL2, CXCL3, CXCL8, and ICAM-1), which is a common pathway for lung epithelial responses to most viral infections.[65] NF-κB is involved in innate and adaptive immunity and is required for resistance to infection.[66] In addition, IL-1, IL-17, and TNF-mediated inflammatory pathways were activated; NOD-like and RIG-I-like receptor signaling were

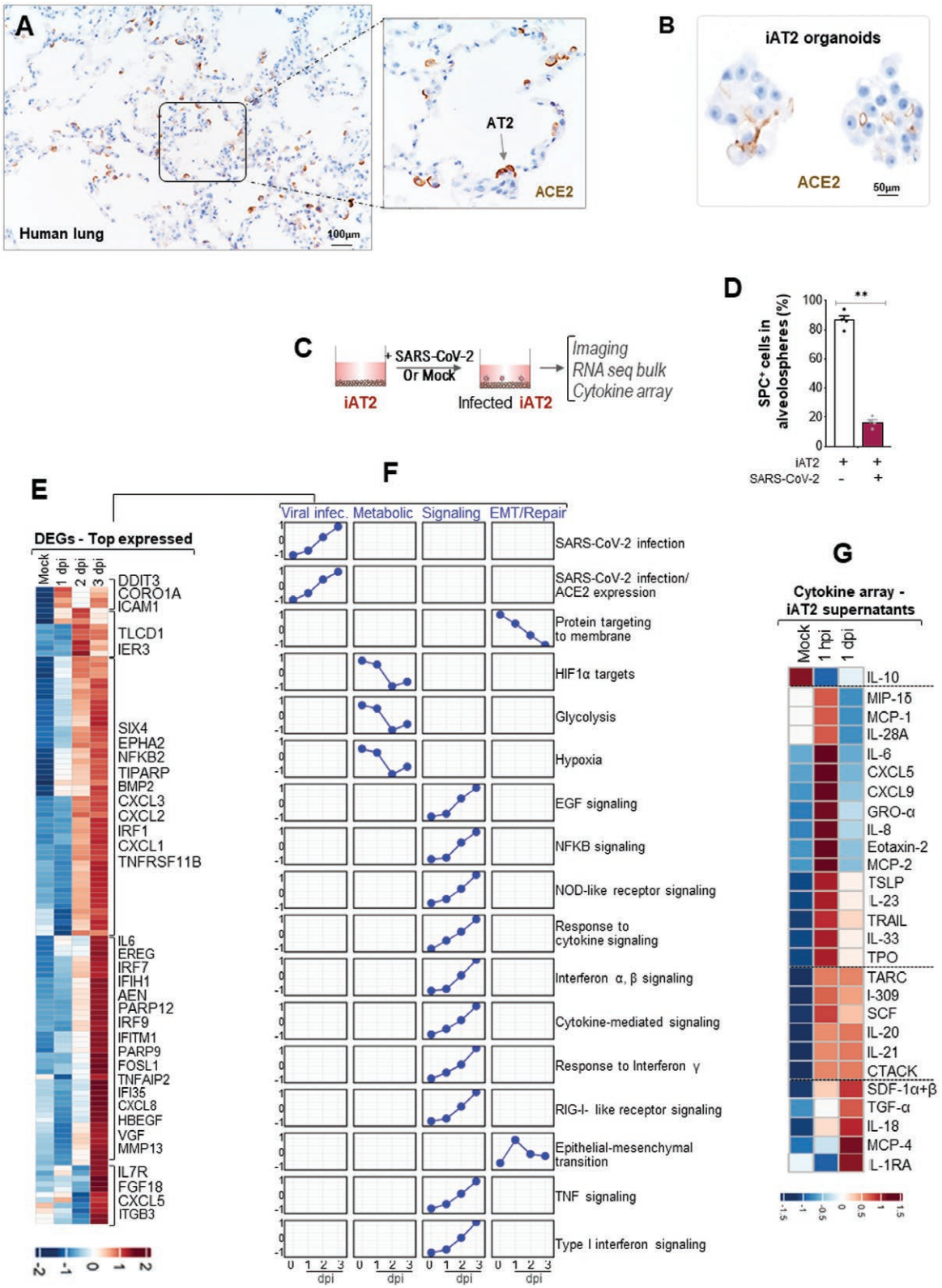

Figure 5. Innate immunity response of iAT2 in SARS-CoV-2 infection. (**A**, **B**) Representative staining for ACE2 in healthy human lung and iAT2 alveolospheres. Scale bar = 100 µm and 50 µm, respectively. (**C**) Schematic of iAT2 alveolospheres infection with SARS-CoV-2. (**D**) Percentage of SPC + alveolospheres before and 24 hours after infection with SARS-CoV-2. (**E**) Heatmap of differentially expressed genes in viral infection class presented in (**F**), between iAT2 and iAT2 infected with SARS-COV-2 after 24 hours. (**F**) Changes in main signaling pathways, cellular function, and cellular compartment in iAT2 alveolospheres before infection and 1, 2, 3 days after infection with SARS-CoV-2 (dpi) analyzed by RNA seq followed by gene set enrichment analysis (GSEA). The mean expression of pathway members were used to plot the bar chart for the selected pathway identified by GSEA. (**G**) Heatmap of cytokines and chemokines in iAT2 alveolospheres before infection and 24 hours after infection with SARS-CoV-2.

also found to be upregulated in infected iAT2 cells. As an alternative fate to SARS-CoV-2-induced cell death (FOS, TNF-mediated apoptosis), infected iAT2 cells showed hallmarks of epithelial remodeling and fibrosis. For example, epidermal growth factor receptor (EGFR) signaling (EPHA2, EREG, HB-EGF) was enriched in SARS-CoV-2-infected iAT2 cells, which is intriguing because of the reported potential for EGFR activation to contribute to fibrosis.[67] Moreover, fibrotic marker transcripts and genes of alternate cell fates (eg, MMP13, VGF, IL-17R, FGF18, and ITGB3) were found to be upregulated in iAT2s specifically, 3 days after infection (Fig. 5E–5F).

Early cytokine profiling confirmed induction of epithelial-derived IL-6, IL-8/CXCL8, IL-28A, MCP-1/2, CXCL5, CXCL9, and alarmins (IL33 and TSLP) as early as 1 hour after SARS-CoV-2 infection (1hpi) (Fig. 5G), which are produced in response to respiratory viral infection.[68] In addition, levels of tumor necrosis factor-related apoptosis-inducing ligand, which is a marker of apoptosis that contributes to an "antiviral state,"[69] was found to be highly expressed at 1 hpi.[68] 24 hours after infection, cytokines associated with repair and remodeling were upregulated [eg, TGF-α, IL-18, MCP-4 (CCL13), IL-20, IL-21, CTACK (CC27), SDF-1, and IL-1RA; (Fig. 5G)].[45,70] TGF-α represents an example of another upregulated EGFR ligand, which is interesting because increased EGFR signaling is associated with SARS-CoV-1-induced fibrosis.[67]

Similar to other published models of SARS-CoV-2 infection,[61,64,71] these experiments captured the upregulation of inflammatory pathways and downregulation of AT2-specific metabolic activity and surfactant production. Thus, this model allows for an exploration of AT2 phenotypical changes after infection. In addition, because SARS-CoV-1 was associated with pulmonary fibrosis, there is concern about a similar process post-COVID-19.[67,72] Although mechanistic data after SARS-CoV-2 infection is currently unavailable, the iAT2 in vitro model provides novel insights into the potential signaling pathways that may be associated with fibrosis post-SARS-CoV-2 infection in patients.

One mechanism that has been hypothesized for increased COPD morbidity and mortality in COVID-19 is the potential for increased ACE2 expression to facilitate SARS-CoV-2 infection and replication.[73] In iAT2 cells, ACE2 and TMPRSS2 were expressed (Fig. 6A), which is consistent with prior reports.[59,61] However, in iAT2 cells cocultured with COPD fibroblasts (iAT2 + CFib), ACE2 gene expression was elevated compared to iAT2 cells cocultured with healthy fibroblasts (iAT2 + HFib) (Fig. 6A–6B). In addition, TMPRSS2 and CSL expression were also higher in iAT2 cocultured with COPD fibroblasts (Fig. 6B), which indicates additional factors that may facilitate SARS-CoV-2 infection in COPD.

To better understand the effect of SARS-CoV-2 infection in the COPD alveolar niche, iAT2 cells were cocultured with healthy and COPD fibroblasts and infected with SARS-CoV-2 (10^4 PFU) in 100 µL of media for 1 h and 24 h (Fig. 6C). Here, cocultured iAT2 with healthy fibroblasts showed 3-fold higher SPC expression compared to cocultured iAT2 with COPD fibroblasts (Fig. 6D). Subsequently, after infection, the number of alveolospheres was significantly decreased in both healthy and COPD alveolospheres (Fig. 6D). This effect was more pronounced in COPD alveolospheres indicating their increased susceptibility to SARS-CoV-2 infection (Fig. 6D). In both iAT2 alveolospheres cocultured with healthy or COPD fibroblasts cytokine responses following SARS-CoV-2 infection (Fig. 6G) confirmed decreased anti-inflammatory mediators (eg, IL-10 and GM-CSF). Factors associated with monocyte, macrophage, and/or neutrophil recruitment (eg, M-CSF, MIP-1δ, IL-8/CXCL8, and CXCL5) were upregulated in both conditions 1 hour after infection; TGF-α and IL-18, which are implicated in remodeling, were detected 24 hours post-infection (Fig 6G). Intriguingly, iAT2 alveolospheres cocultures with healthy fibroblasts maintained higher levels of SCF, SDF-1, IL-16, IL-18, IL-20, IL-21, IL-23 IL-28A, IL-33, and TSLP (Fig. 6G). Unlike healthy alveolospheres, the secretion of these cytokines from COPD alveolospheres was reduced (Fig. 6G). This suggests a potential mechanism for impaired immune responses to SARS-CoV-2 infection in patients with COPD, which may be mediated by COPD fibroblasts contributing to fibrotic remodeling and/or attenuated cytokine secretion.

Next, the relevant biological pathways enriched in healthy and COPD alveolospheres were investigated to predict mechanisms by which COPD is more susceptible to SARS-CoV-2 infection. RNA seq identified DEGs between healthy and COPD cocultures (Fig. 6E and F). Pathway analysis revealed that the main DEGs significantly enriched in iAT2 + CFib included core genes involved in viral infection, signaling pathways, metabolic activity, and remodeling (eg, EMT and repair). Importantly, transcripts levels of MX1 and MX2, which are involved in antiviral responses, were downregulated in COPD alveolospheres (Fig. 6E–6F), and support a mechanism for increased COPD susceptibility to viral infection.[74] Non-infected COPD alveolospheres showed increased IL-6 and CXCL8 transcripts. The genes related to cell metabolism glycolysis, oxidative phosphorylation, and hypoxia were upregulated in iAT2 + CFib, which contribute to energy production and survival.[54,75,76] However hypoxic stress and metabolic dysfunction act as prime modulators of mitochondrial dysfunction and upregulation of oxidative stress-related genes that lead to increased cell death in COPD alveolospheres compared to healthy alveolospheres (Fig. 6E). Macroautophagy and the formation of phagosomes processes, which host cells use to deliver trapped viral cargo to the lysosome for degradation to defend against viral infection,[77] were upregulated in both COPD and healthy alveolospheres. Furthermore, pathways involved in repair, remodeling (eg, Notch, Wnt), and mesenchyme development were significantly upregulated in non-infected COPD alveolospheres compared to both COPD and healthy alveolospheres after viral infection. However, expression of MMP1 and MMP3 were increased in COPD alveolospheres before and after infection. These MMPs cleave extracellular matrix proteins, which contribute to AT2 destruction in COPD. Given that viral infection is the multifaceted intrigue of inflammation and tissue destruction, it is not surprising that genes involved in the repair are downregulated after infection (Fig. 6E–F).[13,76] Thus, via a combination of cytokine and transcriptomic profiling, these data unveiled the altered nature of immune responses against viral infection in COPD alveolospheres, which models increased susceptibility to SARS-CoV-2 infection in COPD.[49,54,78] These aberrant immune responses to viral infection may explain accentuated tissue damage and inflammation in patients with COPD upon SARS-CoV-2 infection.[76]

To verify whether our model recapitulate the alveolar niche response to viral infection, we cross-validate the transcriptomic profiles of our iAT2/healthy Fibroblast

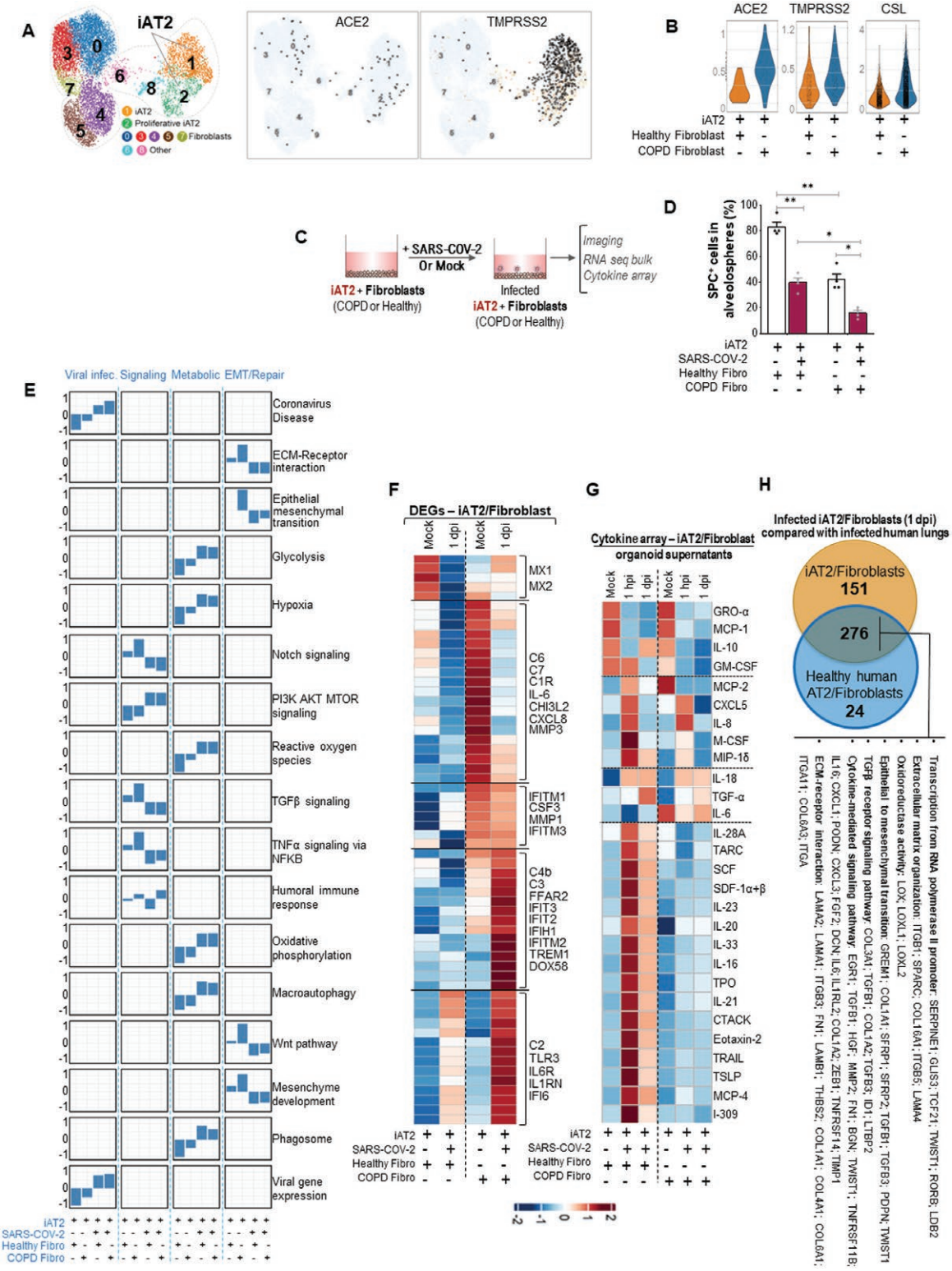

Figure 6. Innate immunity response to SARS-CoV-2 infection in iAT2-based COPD model. (**A**) t-SNE plot of the relative abundance of ACE2 and TMRRSS2 in iAT2 and fibroblast alveolospheres coculture system. (**B**) The expression of ACE2, TMPRSS2, and CSL in iAT2 in iAT2/healthy fibroblasts and iAT2/COPD fibroblasts alveolospheres. (**C**) Schematic of iAT2/Fibroblast alveolospheres (COPD and healthy) infection with SARS-CoV-2. (**D**) Percentage of SPC + alveolospheres before and 24 hours after infection with SARS-CoV-2. Bars represent mean ± SEM, $n = 3$ biological replicates. (**E**) Changes in main signaling pathways, cellular function, and cellular compartment in iAT2/healthy fibroblast and iAT2/COPD fibroblast alveolospheres before and 1, 2, and 3 days after infection with SARS-CoV-2 (dpi) analyzed by RNA seq followed by gene set enrichment analysis (GSEA). The mean expression of pathway members was used to plot the bar chart for the selected pathway identified by GSEA. (**F**) Heatmap of the most differentially expressed genes between iAT2/healthy fibroblast and iAT2/COPD fibroblast alveolospheres before and 24 hours after infection with SARS-CoV-2. (**G**) Heatmap of cytokines and chemokines in iAT2/healthy fibroblast and iAT2/COPD fibroblast alveolospheres before infection and 24 hours after infection with SARS-CoV-2. (**H**) Overlaps between DEGs identified from infected iAT2/fibroblasts (1 dpi v.s. mock) compared with that predicted from AT2/fibroblasts in infected human lung data. Representative pathways enriched by the top-ranked overlapped DEGs were highlighted on the right of the Venn diagram.

coculture at day 1 post-infection with infected human lungs (patients with non-COPD). DEGs of infected cocultures were compared to DEGs of human data after extracting and combining AT2 and fibroblast clusters form single-cell RNAseq data publicly available.[61] Our data revealed that the majority of DEGs in infected human lungs (fibroblast and AT2 clusters) were conserved in our infected organoid cocultures. These DEG are involved in key pathological pathways involved in SARS-CoV-2 infection such as extracellular matrix organization, epithelial to mesenchymal transition, TGFβ signaling pathway, and cytokine-mediated signaling pathways. Although IFN and TNF pathways are expected to be enriched in our overlapped pathway analyses, because they operate as a first line in lung defense against viral infections, we did not see evidence for this in the top-regulated overlapped pathways. This is potentially due to the collection timepoint of infected lungs from deceased SARS-COV-2 patients that might have occurred post-TNF and IFN pathway activation (Fig. 6H).

A Novel Human Antibody Inhibits SARS-COV-2 Infection in iAT2 Cells

iAT2 cells offer an important model system to test and to develop therapeutics.[61] Using iAT2 cells, a novel cellular assay was developed to test the binding and adsorption of SARS-CoV-2 virus. A GFP-expressing lentivirus pseudotyped with viral spike protein (S), which is the molecular determinant of viral attachment, fusion, and entry into host cells, was engineered to monitor the binding of SARS-CoV-2 spike to ACE2 on iAT2s. Two SARS-CoV-2 pseudoviruses were used to mimic viral entry mediated by prototypic and mutant D614G SARS-CoV-2 spike in vitro. High-content imaging with comprehensive image analysis was used to evaluate the potency of mAb binding to S protein (Fig. 7A–D). Incubation of GFP expressing pseudoviruses with iAT2s alveolospheres in suspension cultures for 72 hours resulted in viral binding and infection into iAT2 cells, which was confirmed by measuring GFP expression (Fig. 7A-D). Next, a neutralizing mAb to SARS-CoV-2 S protein (CVH5 or AZD7442) was tested to investigate the potential to decrease GFP-expressing pseudovirus infection of iAT2 cells.[79] In these experiments, CVH5 significantly prevented the entering of GFP-pseudovirus into iAT2 cells. In addition, CVH5 remained broadly effective against mutated (D614G mutation) SARS-CoV-2 pseudovirus (Fig. 7E–7F).

We next tested the protective efficacy of mAbs using COPD (iAT2 + CFib) and healthy (iAT2 + HFib) alveolospheres. Exposure of COPD and healthy alveolospheres to GFP-pseudoviruses for 72 hours resulted in higher binding/adsorption of virus to COPD alveolospheres which was confirmed by measuring GFP expression (Fig. 7G). Treatment with CVH5 mAb inhibited GFP-pseudoviruses entering into COPD and healthy alveolospheres. In contrast, high levels of GFP-pseudovirus were observed in the isotype control-treated alveolospheres (Fig. 7G). Collectively, CVH5 studied here suggests that neutralizing mAbs are promising candidates for prevention or treatment of COVID-19. Importantly, these results show the potential for a physiologically relevant in vitro model to investigate the effectiveness of our antibodies against SARS-CoV-2 that will contribute to the development of monoclonal therapeutic antibodies.

Discussion

Chronic obstructive pulmonary disease (COPD) is characterized by chronic inflammation and the destruction of lung alveolar-mesenchymal units.[80] However, the dynamic changes in cellular structure and composition of the alveolar-mesenchymal units in COPD lungs remain incompletely characterized.[50,81] Human iPSCs-derived cells provide a novel in vitro patient-specific model to investigate changes in alveolar epithelial function in health and disease.[82] To further decipher molecular mechanisms regulating AT2 function in COPD, we developed alveolospheres of iAT2 cells coculture with human primary lung fibroblasts. This system has the potential to provide deeper mechanistic insights into the extensive mesenchymal-epithelial crosstalk involved in the alveolar niche,[13,14,26] and to explore normal and pathologic paracrine cues influencing alveolar development in health and disease.[36]

At the outset, the in vitro coculture system confirmed prior observations that the development of human AT2 epithelium depends on fibroblast-AT2 epithelial cell crosstalk in the alveolar-mesenchymal microenvironment that is regulated by oscillations of canonical Wnt, AREG, EGF, and FGF signaling.[14,24,25,32,35] Using proteomic and sc-RNA seq approaches, the cellular and molecular landscape in aloveosphere cocultures identified 5 subtypes of fibroblasts with distinct expression patterns. Healthy fibroblasts (Clusters 3 and 7) exhibited increased expression of trophic factors required for iAT2 growth to support the alveolar niche. Previously, such trophic factors were shown to be required for a subpopulation of AT2 cells with stem cell activity (Axin2 + cells) to contribute to alveolar regeneration and remodeling. Prior studies described trophic factors (eg, Wnt and FGF) that are produced by fibroblasts in close proximity to individual AT2 cells in human lungs.[26,35,40] COPD fibroblasts (Clusters 0, 4, and 5) displayed higher levels of pro-fibrotic mediators including TGFβ and Wnt5a. TGFβ signaling was shown to be a significant driver of AT2 fate changes during epithelial-mesenchymal transition in COPD,[76,83] while altered Wnt signaling in fibroblasts located in close proximity to AT2 cells was reported to modulate pathological changes in COPD alveolar epithelium. Sustained Wnt5a secretion by COPD fibroblasts induces AT2 stem cells (Axin2 + AT2) depletion and impairs alveolar regeneration in diseased lungs.[25,83,84] The COPD fibroblasts (Clusters 0, 4, and 5) also showed evidence for decreased trophic factor production and increased pro-inflammatory cytokine expression, which has the potential to promote inflammation, fibrosis, and apoptosis in COPD and has been described previously[24]. However, the iAT2 coculture model broadens the mechanistic understanding of the source and effect of these cytokines.

Pathway analyses confirmed that COPD fibroblasts expressed pathological signaling pathways that may function via autocrine or paracrine signaling to impair AT2 function(s) by activating or accelerating cell aging and senescence, inflammation, fibrosis, and apoptosis in iAT2 cells. iAT2 cells cocultured with COPD fibroblasts showed increased IL6, mTOR, and NFKB signaling, which represent molecules and inflammatory pathways that are consistently associated with COPD pathogenesis.[50,53] In addition, these experiments identified mediators secreted by COPD fibroblasts that may trigger mitochondrial dysfunction, alteration of extracellular matrix organization, and activation of epithelial-mesenchymal transition in AT2 cells.[50,53] To complement

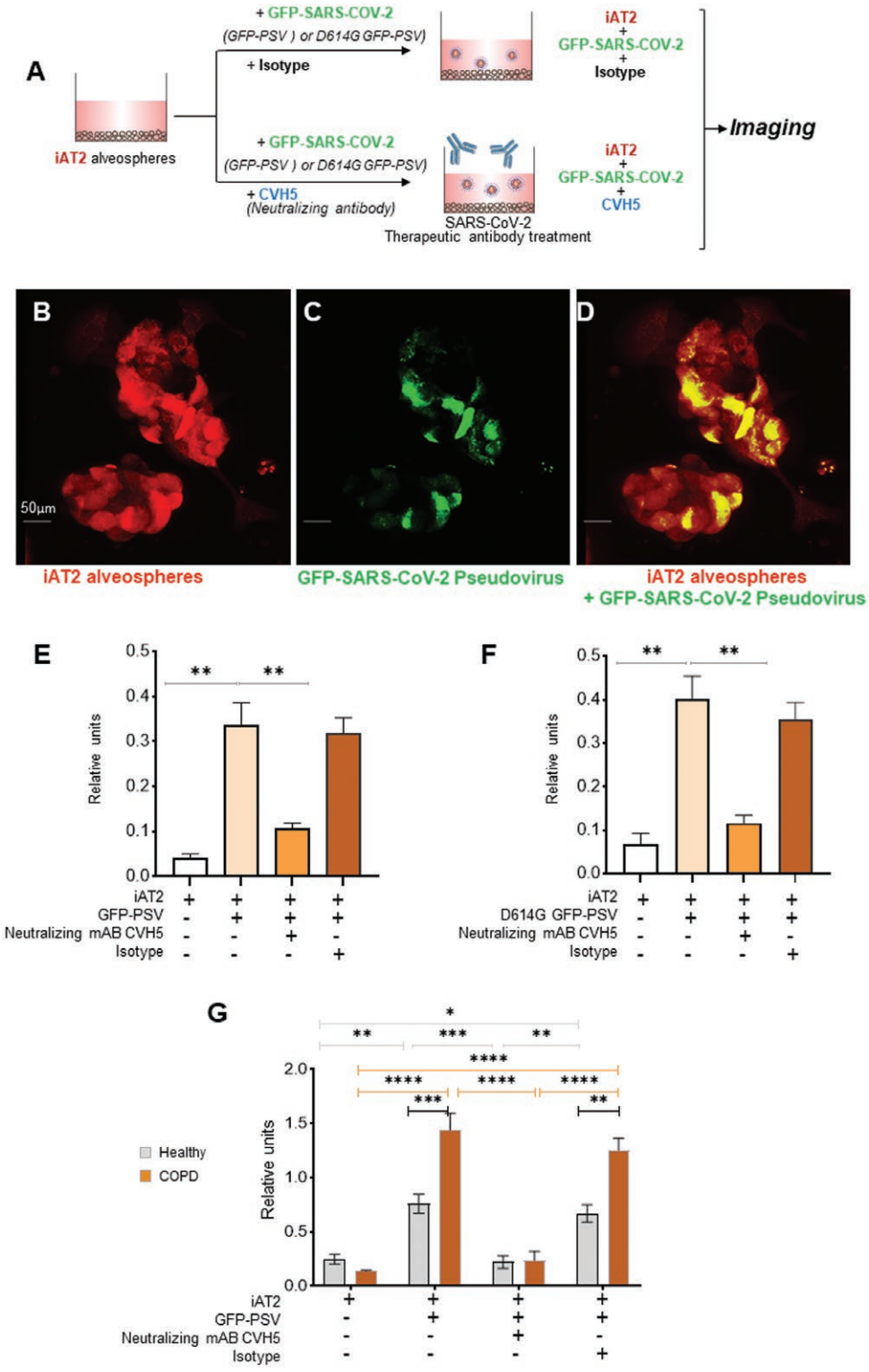

Figure 7. Functional evaluation of neutralizing SARS-CoV-2 monoclonal therapeutic antibody (mAbs) in iAT2 alveolospheres. (**A**) Schematic of infection of iAT2 alveolospheres with SARS-CoV-2 in the presence or absence of neutralizing antibody or controls. (**B-D**) immunofluorescence of iAT2 alveolospheres infected with SARS-COV2. (B) iAT2 alveolospheres, red shows SPC reporter. (C) infection of iAT2 alveolospheres with GFP-expressing SARS-CoV-2 pseudovirus. (D) Merged of SPC-positive cells with SARS-COV2 infected cells. Scale bars = 50 μm. (**E**) Efficacy of neutralizing human mAB (CVH5) against GFP expressing SARS-CoV-2 pseudovirus (GFP-PSV) infection in iAT2 cells in vitro. Bars represent mean ± SEM, $n = 5$ replicates. (**F**) Efficacy of CVH5 against mutant SARS-CoV-2 infection (D614G GFP-PSV) in iAT2 cells in vitro. Bars represent mean ± SEM, $n = 5$ replicates. (**G**) Efficacy of CVH5 against GFP-SARS-CoV-2 pseudovirus (GFP-PSV) infection in healthy (iAT2 + HFib) and COPD (iAT2 + CFib) alveolospheres in vitro. Bars represent mean ± SEM, $n = 5$ replicates.

these experiments, cytokine analysis provided additional novel evidence for the contribution of paracrine signaling pathways within the alveolar niche in vitro. Cytokine profiling experiments highlighted the abundant production of SASP and proinflammatory cytokines (eg, IL-6, IL-8/CXCL8, and TNFα) in COPD alveolospheres or ALI cultures. In addition, these experiments showed reduced secretion of host defense mediators, such as IL-10.[52] These results suggest that a combination of exaggerated inflammation coupled with impaired immune responses contributes to lung damage and recurrent infections in COPD.[41,42,44,49]

These experiments identified the critical role that fibroblasts contribute in the model of the alveolar-mesenchymal niche. The addition of disease-specific fibroblasts further elucidated the contribution of COPD fibroblasts, mediated by changes in cellular expression and secreted cytokines, to alter AT2 function. Therefore, we hypothesized that the iAT2-fibroblast cocultures would provide a detailed understanding of iAT2-fibroblast interactions in COPD during SARS-CoV-2 infection to improve our understanding of viral pathogenesis, and to unravel phenotypic changes and molecular mechanisms. In response to SARS-CoV-2 infection. Our data highlighted the loss of iAT2s that was associated with an enrichment in inflammatory signaling and cytokine production, which may help to explain the diffuse alveolar damage observed in patients with COVID-19.[23,30,45,70,75,85] Consistent with previous studies, innate immune signaling and anti-viral immunity, which includes interferon (IFN)[61] and NF-kB[66] signaling, were upregulated in SARS-CoV-2 alveolospheres. Indeed, this model captured the gradual decline of AT2-specific signaling, such as downregulation of metabolic activity and surfactant production, as SARS-CoV-2 induced AT2 cell apoptosis, which provided evidence for productive viral infection that drives host translational machinery to produce products required for viral replication and packaging. These metabolic changes may aid AT2 cell survival during infection.[62] In addition, activation of epithelial remodeling and fibrosis were upregulated in virus-infected iAT2 alveolospheres that include EGFR signaling (EPHA2, EREG, HB-EGF, and TGFα) and markers of mesenchymal cell fate progression (MMP13, VGF, IL-17R, FGF18, and ITGB3). These results suggest that AT2 cells are responding to SARS-CoV-2 to activate pathways that contribute to altered wound healing, epithelial-mesenchymal transition and fibrosis.[67] More importantly, the iAT2 model offers a comprehensive characterization of epithelial remodeling and fibrosis pathways that may contribute to the increased severity of COPD observed during the COVID-19 pandemic.[67,72]

Next, the AT2-mesenchymal-unit was modeled using iAT2 alveolospheres cocultured with COPD or healthy fibroblasts and challenged with SARS-CoV-2 infection. The result was a decrease in anti-inflammatory mediators (ie, IL-10, GM-CSF) in healthy and COPD alveolospheres with an expected increase in monocyte/macrophage and neutrophil chemokines, which were upregulated as early as 1h after infection. However, factors associated with remodeling (eg, TGF-α and IL-18) were produced 24 hours post-infection. Unlike healthy alveolospheres, the epithelial-derived cytokines (ie, IL-33 and TSLP) were found reduced in COPD alveolospheres after viral infection. This reduction may reflect either the increased capture of those mediators by COPD fibroblasts undergoing fibrotic remodeling or the attenuated cytokine secretion that could be attributed to either increased AT2 death or the inhibitory effect of fibroblast on epithelial secretion; thus arguing for the impaired immune defenses to SARS-CoV-2 infection in COPD alveolar niche.

RNA seq was used to characterize the relevant biological pathways enriched in COPD alveolospheres that may predict the pathological mechanisms related to COPD susceptibility to SARS-CoV-2 infection. Here, we found distinct core genes involved in viral infection, signaling pathways, metabolic activity and remodeling (EMT/repair) that were significantly enriched in COPD alveolospheres. Interestingly, MX1 and MX2, which are IFN-dependent genes associated with antiviral immunity were downregulated,[74] while interferon signaling was upregulated. While this result confirms the observation that IFN signaling is exaggerated in response to SARS-CoV-2 infection, it identifies a novel mechanism in COPD for impaired antiviral immunity.

Altered cell metabolism (glycolysis, oxidative phosphorylation) in COPD alveolospheres contributes to energy production[54,75,76] that may result in mitochondrial dysfunction that triggers increased COPD AT2 cell death, which is exacerbated by hypoxia. Further examination of repair/remodeling pathways identified significantly upregulated Notch and WNT signaling, as well as mesenchyme development pathways in non-infected COPD alveolospheres, which were downregulated after viral infection and suggests a mechanism for viral infection to activate AT2 cell death as an alternative to changes in cell fate/remodeling. Collectively, this data elucidated the altered immune responses to viral infection in COPD alveolospheres, which provides mechanistic insights into host responses in COPD to SARS-CoV-2 infection,[49,52,54] and increased tissue damage and inflammation observed in patients with COPD in the COVID-19 pandemic.[76]

An exciting aspect of the COPD iAT2-fibroblast model is the contribution to developing neutralizing monoclonal antibodies (mAbs) that bind to wild-type and mutant SARS-CoV-2 viruses to prevent infection. Indeed, the iAT2 alveolospheres represent a sophisticated system to functionally evaluate the mAbs potency to prevent viral attachment and internalization into AT2 cells. Using live imaging of infected alveolospheres, this model provided evidence that neutralizing mAb (CVH5) inhibited SARS-CoV-2 pseudovirus attachment and internalization into iAT2 cells. In addition, CVH5 studied in COPD alveolospheres offers resistance to SARS-CoV-2 in COPD and sets the stage for evaluation of mAbs as candidates for use as COVID-19 preventative immunotherapeutic in reducing the viral burden and inflammation in most vulnerable patients in a disease-specific model.[79,86,87]

In summary, the iAT2 alveolospheres represent a sophisticated in vitro stem cell-based system to model disease mechanisms and to investigate characteristics of viral infection in the alveolar-mesenchymal niche. These data highlight the valuable application of iAT2 alveolospheres to model the specific contribution of different cell types to COPD pathogenesis. Given that our iAT2-healthy fibroblasts coculture system was able to recapitulate the cellular responses to SARS-COV-2 infection of human healthy lungs, we anticipate that our emphysema model might predict the alveolar niche's response to viral infection in patients with COPD. More importantly, this system was shown to provide a promising tool to investigate and to develop therapeutics that may be influenced by pathophysiologic responses in the human alveolar niche. Future experiments will incorporate immune cells (eg, macrophages and neutrophils), which have a role in

COPD pathogenesis, and may improve our understanding of the inflammatory modality in the alveolar niche. In addition, the observation that iAT2s do not differentiate into type 1 alveolar cells (AT1) is a limitation that has been previously reported in vitro for both iPSC-derived and primary human AT2s.[15,61] However, ongoing studies are investigating the contribution of fibroblasts to influence iAT2 alveolospheres to differentiate into AT1.

Materials and Methods

Culture of Human Induced Pluripotent Stem Cells (iPSC)

The BU3 NGST iPSC line used in this study was generously provided by Dr. Darrell N. Kotton. These cells were cultured on Matrigel in mTesR medium, with daily medium changes. Undifferentiated iPSCs were passaged onto fresh Matrigel every 4-5 days.

Differentiation of iPSC to Lung Progenitor Cells and Alveolar Type 2 (iAT2) Cells

The iPSCs were differentiated into lung progenitor cells and iAT2 cells using a modified differentiation protocol.[15,22] STEMdiff Definitive Endoderm Kit (STEMCELL Technologies) was used to induce definitive endoderm following the manufacturer's protocol. After approximately 72-84 hours, cells were harvested and analyzed by flow cytometry to confirm the efficiency of definitive endoderm induction [CD117 and CXCR4 double-positive cell markers[22,88]]. After definitive endoderm induction, cells were dissociated into small clumps and passaged 1:6 on matrigel-coated plates in serum-free differentiation medium (SFDM) [IMDM/F12 (1:3) (Life Technologies)], N2 (Life Technologies), B27, 50 µg/mL ascorbic acid, 2 mM Glutamax, 0.4 µM monothioglycerol, 0.05% BSA supplemented with 2 µM dorsomorphin (Sigma-Aldrich) and 10 µM SB431542 (Tocris) for 72 hours. Y-27632 (10 µM, Tocris) was added for the first 24 hours only.[88]

For induction of early-stage lung progenitor cells, anterior foregut endoderm was cultured in SFDM supplemented with 3 µM CHIR99021 (Tocris), 10 ng/mL rhBMP4 (R&D Systems), and 50–100 nM retinoic acid (Sigma-Aldrich). Medium was changed every other day for 8-9 days.[88]

To generate iAT2 alveolospheres, on day 15 of differentiation progenitor cells were dissociated with 0.05% trypsin (Thermo Fisher Scientific) and sorted for NKX21$^+$ cells. Sorted cells were suspended in growth factor reduced Matrigel at 400 cells/µL density. A total of 50 µl Matrigel droplets were seeded in 6 well plates and incubated at 37 °C for 30 minutes. Once Matrigel solidified, 2-3 mL differentiation medium containing SFDM supplemented with 3 µM CHIR99021, and 10 ng/mL rhKGF, 50 nM dexamethasone (Sigma-Aldrich), 0.1 mM 8-bromoadenosine 3′,5′-cyclic monophosphate (8-Br-cAMP) sodium salt (Sigma-Aldrich), and 0.1 mM 3-isobutyl-1-methylxanthine (IBMX) (Sigma-Aldrich), henceforth called alveolospheres medium, was added to each plate. Y-27632 (10 µM) was added for the first 48 hours. Medium change is completed every 48 hours for 2 weeks.[15] For viral infection and mABs experiments, alveolospheres were released from Matrigel. Droplets were incubated in dispase (2 mg/mL, Fisher) at 37 °C for 1 hour, centrifuged at 300 *g* for 1 minute, washed in 1× PBS, and centrifuged again at 300 × *g* for 1 minute.

Co-Culture of Fibroblast and iAT2 Cells

Fibroblasts from healthy and COPD donors were generously provided by Dr. Mauricio Rojas (Ohio State University) for coculture experiments with iAT2 cells in 3D alveolospheres or ALI cultures (Table 1). For fibroblast cocultures, alveolospheres were dissociated into a single-cell suspension. iAT2 cells and fibroblasts were cocultured (1:5 ratio) in 3D system. iAT2 and fibroblast cell mixtures were thoroughly mixed in 100% growth factor reduced Matrigel (Corning, 354234) in ice. A total of 50 µl Matrigel droplets containing 5×10^4 cells were plated (6-well plate) and incubated at 37 °C for 30 minutes. Once Matrigel solidified, 2-3 mL of aloveosphere medium was added to each well. After 2 weeks cell culture supernatants were collected for cytokine analysis and cells were collected for sc-RNA-seq. For ALI cultures, iAT2 cells were transferred into Matrigel pre-coated TransWell inserts (Corning) at 500 000 cells/cm^2. After 1 week, upon formation of a confluent iAT2 cell layer, the apical culture medium was removed, and filter inserts were transferred to 12 well plates containing fibroblasts. Coculture was performed for 7 days with healthy and COPD fibroblasts. Medium and cells from these cultures were collected at the end of 7 days of coculture for cytokine and gene expression analysis.

Staining and Imaging of iAT2 in Aloveosphere and ALI Culture

Organoid and ALI of iAT2 cultures were fixed in 10% neutral buffered formalin for 24 hours and embedded in paraffin. Paraffin sections (4 µm) were mounted on positively charged slides and stained on the Ventana Discovery Ultra with a sequential 3 plex chromogenic assay. Antigen retrieval was done with cell conditioner 1 and endogenous peroxidase was blocked with discovery inhibitor for 12 minutes. Anti-ACE2 (Abcam, ab108252) was applied for 40 minutes at 36 °C and visualized with mouse anti-HQ (12 minutes) and anti-HQ HRP (12 minutes), and incubated in the DAB substrate (8 minutes). The stained slides were rinsed with Dawn detergent, counterstained with hematoxylin, rinsed, dehydrated with a graded series of ethanol, and xylene and mounted with permanent mounting media. A confocal microscope was used for live 3D imaging of alveolospheres and ALI culture to quantify SPC expression. The Green channel was set to capture a signal from NKX2.1$^+$ cells, and a red channel was used to capture SPC$^+$ cell signals. The ratio of green fluorescent volume to red fluorescent volume was used to evaluate SPC expression in organoids and ALI cultures using Imaris software.

Table 1. Mean age, sex, and smoking history of COPD and healthy donors.

	COPD (n = 10)	Healthy (n = 10)
Age (years)	58.5	44.3
Sex (male)	10 (6)	10 (7)
Cigarette smoking		
Current smoker	3	0
Ex-smoker	6	1
Non-smoker	1	9

Generation of S Protein Pseudotyped Lentivirus

A codon-optimized cDNA sequence encoding SARS-CoV2 Spike protein with a deletion in its C-terminal 19 amino acid residues for better pseudo-typing was synthesized by GenScripts and cloned in a mammalian expression plasmid downstream of a CAG promoter. COVID S-pseudo typed lentivectors were produced by transient transfection of suspension 293 cells with this COVID S expression plasmid, 2 packaging plasmids encoding HIV GagPol and HIV Rev, along with GFP- or luciferase-expressing lentiviral genome plasmid. Virus supernatants were harvested 3 days after transfection, passed through a 0.45 µm-pore-sized filter, and concentrated 100-fold by ultracentrifugation.

SARS-CoV-2 Viral Infection of iAT2 Alveolospheres

SARS-CoV-2 isolate USA-WA1/2020 used for in vitro experiments was obtained from BEI reagent repository and propagated and tittered in Vero E6 cells as described previously.[89] All infection experiments were performed in a Biosafety Level 3 facility, licensed by the State of Connecticut and Yale University. Alveolospheres were extracted from Matrigel and were mixed with 10^4 plaque-forming units (PFU) of SARS-CoV-2 in 100µ total volume of iAT2 medium. Virus inoculation of alveolospheres ($n = 3$) was completed for 1 hour at 37 °C. After productive viral infection, alveolospheres were collected in 15 mL tubes and were washed with medium to remove unbound virus. Fresh medium was added to alveolospheres and re-plated in a new low attachment plate. Supernatants were collected after infection for cytokines analysis and cell lysates were stored at −80 °C for RNA sequencing.

Neutralization Tests of SARS-CoV-2 Specific mAb in iAT2 Alveolospheres

iAT2 alveolospheres were extracted from Matrigel and infected with GFP-expressing pseudovirus expressing prototypic (GFP-PSV) or D614G variant SARS-CoV-2 spike (D614G GFP-PSV). Alveolospheres were cultured in media without CHIR99021 throughout the experiment to minimize GFP expression from NKX21$^+$ iAT2 cells. Pseudo-virus and mutant virus were suspended in a cell culture medium and were added to iAT2. The virus-infected alveolospheres mixtures were transferred to a low attachment plate and were treated with CVH5 (SARS-CoV-2 specific neutralizing mAb) or isotype control ($n = 4$) [both manufactured at AstraZeneca, Gaithersburg, MD[79]]. For dose-response assays, serial 3-fold dilutions starting at 10 µg/mL purified mAbs were applied to iAT2 wells in triplicate. The plate was incubated for 4 hours at 37 °C and imaged by Zeiss LSM800 confocal microscope after 96 hours. The ratio of green fluorescent volume (GFP expressing pseudo-virus) to the red fluorescent volume (SPC-positive cells) was used to evaluate the binding of virus to the iAT2 alveolospheres and mAb binding to S protein in GFP-pseudo-virus.

Cytokine and Chemokine Analysis

Supernatants from all experiments were aliquoted and stored at −80 °C. Media were shipped to Eve Technologies on dry ice. The level of cytokines and chemokines were measured from media using Human cytokine Array/Chemokine Array 71-403 Plex Panel (HD71) after the first thaw. Heatmap visualization was built with ComplexHeatmap using the mean natural logarithm of the readouts from 3 technical replicates, centered and scaled by their SD. The assay readouts that deviated from the median at least twice the average intervals between any technical replicates of the same sample were treated as outliers and excluded from the analysis.

RNA Isolation, RNA-Sequencing, and Bioinformatics Analysis

RNA Isolation

Total RNA was extracted from alveolospheres and ALI cultures using RNeasy Mini kit (Qiagen, Hilden, GER) following the manufacturer's instructions and quantified with a NanoDrop Spectrophotometer (Thermo Fisher Scientific). For the low amount of samples PicoPure RNA isolation kit (applied biosystems) was used to isolate RNA following the manufacturer's instruction.

RNA Sequencing

The concentration of extracted RNA was determined by Qubit RNA HS Assay kit (Thermo Fisher Scientific), and their integrity was checked by High Sensitivity RNA ScreenTape Analysis (Agilent). Human ribosomal RNA was depleted with NEBNext rRNA Depletion Kit v2 (New England Biolab), and libraries were prepared with NEBNext Ultra II Directional RNA Library Prep Kit for Illumina (New England Biolab) following manufacturer's recommendation. The size distribution and concentration of libraries were determined by High Sensitivity D1000 ScreenTape Assay (Agilent) and KAPA Library Quantification Kits (Roche). All libraries were normalized to 1.5 nM, pooled together evenly, and sequenced on an Illumina NovaSeq 6000 sequencer using NovaSeq 6000 S1 Reagent Kit (200 cycles) with 2 × 100 bp paired-end reads.

Single-Cell Sequencing

To generate single-cell suspensions, alveolospheres were incubated in 0.05% trypsin and continued through the trypsin-based dissociation protocol described above. After cell density was determined by cell counter, 16 000 cells per sample were loaded onto Chromium Single Cell Controller (10X Genomics) and libraries were prepared with Chromium Single-cell 3′ Reagent Kits V3 chemistry (10X Genomics) following the manufacturer's recommendation. The size distribution and concentration of libraries were determined by High Sensitivity D1000 ScreenTape Assay (Agilent) and KAPA Library Quantification Kits (Roche). All libraries were normalized to 1.5 nM, pooled together evenly and sequenced on an Illumina NovaSeq 6000 sequencer using NovaSeq 6000 S1 Reagent Kit (100 cycles) with 10X Genomics' recommended read-length settings.

Bioinformatic analysis: CellRanger 3.0 was used to convert fastq files into raw counts for single-cell analysis. Seurat v3.0 was used for individual sample QC and filtering with customized R script (v 3.6). Scanpy v1.4.6 was used for data integration as well as downstream data analysis visa customized python script. Significant pathways were considered those with Benjamini–Hochberg false discovery rate-adjusted P-value (FDR) < .1.

Gene-level counts were computed by the bulk RNA-seq workflow implemented in bcbio-nextgen framework v1.1.5 (https://bcbio-nextgen.readthedocs.org.[90]; In this workflow, raw sequencing reads were aligned to Genome Reference Consortium Human Build 38 (hg38) by hisat2 aligner v

2.1.0 (Kim et al, 2019). MultiQC v1.7[91] was used to assess the quality of sequencing reads based on their counts, lengths, composition, and distribution on the genome. Gene counts were normalized to log base 2 of count per million reads mapped (cpm) with edgeR v3.28.1. Differential gene expression (DGE) analysis was performed using edgeR and Ensembl gene annotation (release 99) to assess the changes in each experiment condition relative to the control (eg, mock infection). Only the genes with 1 cpm or greater for at least 2 samples were kept for the analysis.

To compare our data to publicly available data, DEGs between 2 cell subpopulations of single-cell RNA-sequencing (scRNA-seq) data were identified using the FindMarker function in Seurat v.4.0.5 with the default Wilcoxon rank sum test except for DEGs on fibroblast, on which likelihood-ratio test was used. DEGs on bulk level were identified using DESeqv.1.34.0. We required the following criteria to obtain the DEGs. First, the gene expression between the 2 cell subpopulationsis statistically significant with a false discovery rate (FDR) <0.05. Second, the expression fold change between the 2 cell subpopulations is greater than zero. Venn diagrams were used to exhibit the overlapped DEGs between our data and public data.

To identify the biological pathways perturbed in the experiment conditions, the genes were ranked by their fold changes and subjected to gene set enrichment analysis using fgsea v1.18.0[92] called from ClusterProfiler v4.0.0[93,94] against public annotation resources, including KEGG,[95] Reactome,[96] Gene Ontology,[97] and Molecular Signatures Database (MSigDB).[98] The annotation was assigned if Benjamini–Hochberg adjusted *P*-value ≤ .05. To visualize the overall changes in a significant pathway, the mean expression levels of the pathway members, centered, and scaled by the SD for each gene, were used to construct bar or line charts using ggplot2 v3.3.3 (Wickham, 2009). Heatmap visualization was built with ComplexHeatmap v2.8.0.[99]

Acknowledgments

We thank our colleagues from AstraZeneca, CPPS for immunostaining, Ken Grime and Maria Belvisi for financial support. This work was supported by AstraZeneca R&D and NIH grants K08 AI128043 (CBW), Burroughs Welcome Fund Career Award for Medical Scientists (CBW), Ludwig Family Foundation (CBW), Mathers Charitable Foundation (CBW), Emergent Ventures Fast Grant (CBW, DvD).

Conflict of Interest

All authors except Aigul Moldobaeva, Elise Gubbins, Mia Alfajaro, Craig Wilen, Finn Hawkins, Yang Li, Lori Clarke, Charles Brown, Roland Kolbeck, Qin Ma, Ken Grime, Mauricio Rojas, Jonathan Koff, and Mahboobe Ghaedi are/were employed by and are shareholders of AstraZeneca.

Author Contributions

R.D.: conception and design, laboratory experiments, and data collection, manuscript writing. A.M., E.G., S.C., M.M.A.: conception and design, laboratory experiments, and data collection. C.B.W.: designed and supervised research, financial support. F.H.: designed and supervised research. X.Q., C.C.C.: data analysis and interpretation. Y.L.: data analysis and interpretation. L.C., Y.I.: designed and tested the GFP-pseudovirus. C.B.: laboratory experiments, and data collection. R.K.: financial support. Q.M.: data analysis and interpretation. M.R.: designed and supervised research. J.L.K.: designed and supervised, manuscript writing. M.G.: designed and supervised, manuscript writing, financial support. All authors reviewed and approved the final manuscript.

Data Availability

The data underlying this article will be shared on reasonable request to the corresponding author.

Supplementary Material

Supplementary material is available at *Stem Cells* online.

References

1. Agustí A, Hogg JC. Update on the pathogenesis of COPD reply. *N Engl J Med*. 2019;381(25):2484. https://doi.org/10.1056/NEJMc1914437
2. Pouwels SD, Zijlstra GJ, van der Toorn M, et al. Cigarette smoke-induced necroptosis and DAMP release trigger neutrophilic airway inflammation in mice. *Am J Physiol Lung Cell Mol Physiol*. 2016;310(4):L377-L386. https://doi.org/10.1152/ajplung.00174.2015
3. Hui KPY, Cheung MC, Perera R, et al. Tropism, replication competence, and innate immune responses of the coronavirus SARS-CoV-2 in human respiratory tract and conjunctiva: an analysis in ex-vivo and in-vitro cultures. *Lancet Respir Med*. 2020;8(7):687-695.
4. Farkas L, Farkas D, Warburton D, et al. Cigarette smoke exposure aggravates air space enlargement and alveolar cell apoptosis in Smad3 knockout mice. *Am J Physiol Lung Cell Mol Physiol*. 2011;301(4):L391-L401. https://doi.org/10.1152/ajplung.00369.2010
5. Kulkarni T, O'Reilly P, Antony VB, Gaggar A, Thannickal VJ. Matrix remodeling in pulmonary fibrosis and emphysema. *Am J Respir Cell Mol Biol*. 2016;54(6):751-760. https://doi.org/10.1165/rcmb.2015-0166PS
6. Togo S, Holz O, Liu X, et al. Lung fibroblast repair functions in patients with chronic obstructive pulmonary disease are altered by multiple mechanisms. *Am J Respir Crit Care Med*. 2008;178(3):248-260. https://doi.org/10.1164/rccm.200706-929OC
7. Harrington H, Cato P, Salazar F, et al. Immunocompetent 3D model of human upper airway for disease modeling and in vitro drug evaluation. *Mol Pharm*. 2014;11(7):2082-2091. https://doi.org/10.1021/mp5000295
8. Yi F, Liu GH, Izpisua Belmonte JC. Human induced pluripotent stem cells derived hepatocytes: rising promise for disease modeling, drug development and cell therapy. *Protein Cell*. 2012;3(4):246-250. https://doi.org/10.1007/s13238-012-2918-4
9. Zhang R, Zhang LH, Xie X. iPSCs and small molecules: a reciprocal effort towards better approaches for drug discovery. *Acta Pharmacol Sin*. 2013;34(6):765-776. https://doi.org/10.1038/aps.2013.21
10. Hoegger MJ, Fischer AJ, McMenimen JD, et al. Cystic fibrosis Impaired mucus detachment disrupts mucociliary transport in a piglet model of cystic fibrosis. *Science*. 2014;345(6198):818-822.
11. Scholte BJ, Davidson DJ, Wilke M, Hr DJ. Animal models of cystic fibrosis. *J Cyst Fibros*. 2004;9(2):183-90. https://doi.org/10.1016/j.jcf.2004.05.039
12. Liu C, Oikonomopoulos A, Sayed N, Wu JC. Modeling human diseases with induced pluripotent stem cells: from 2D to

3D and beyond. *Development (Cambridge, England)*. 2018: 8;145(5):dev156166. https://doi.org/10.1242/dev.156166
13. Strikoudis A, Cieślak A, Loffredo L, et al. Modeling of fibrotic lung disease using 3D organoids derived from human pluripotent stem cells. *Cell Rep*. 2019;27(12):3709-3723.e5. https://doi.org/10.1016/j.celrep.2019.05.077
14. Dye BR, Hill DR, Ferguson MA, et al. In vitro generation of human pluripotent stem cell derived lung organoids. *eLife*. 2015;4:e05098.
15. Jacob A, Morley M, Hawkins F, et al. Differentiation of human pluripotent stem cells into functional lung alveolar epithelial cells. *Cell Stem Cell*. 2017;21(4):472-488.e10. https://doi.org/10.1016/j.stem.2017.08.014
16. McCauley KB, Hawkins F, Serra M, et al. Efficient derivation of functional human airway epithelium from pluripotent stem cells via temporal regulation of Wnt signaling. *Cell Stem Cell*. 2017;20(6):844-857.e6. https://doi.org/10.1016/j.stem.2017.03.001
17. Huang SX, Islam MN, O'Neill J, et al. Efficient generation of lung and airway epithelial cells from human pluripotent stem cells. *Nat Biotechnol*. 2014;32(1):84-91. https://doi.org/10.1038/nbt.2754
18. Doss MX, Sachinidis A. Current challenges of iPSC-based disease modeling and therapeutic implications. *Cells*. 2019;8(5):403. https://doi.org/10.3390/cells8050403
19. Han Y, Yang L, Duan X, et al. Identification of candidate COVID-19 therapeutics using hPSC-derived lung organoids. *bioRxivbiology*. 2020:2020.05.05.079095. https://doi.org/10.1101/2020.05.05.079095
20. Shi Y, Inoue H, Wu JC, Yamanaka S. Induced pluripotent stem cell technology: a decade of progress. *Nat Rev Drug Discov*. 2017;16(2):115-130. https://doi.org/10.1038/nrd.2016.245
21. Takahashi K, Tanabe K, Ohnuki M, et al. Induction of pluripotent stem cells from adult human fibroblasts by defined factors. *Cell*. 2007;131(5):861-872. https://doi.org/10.1016/j.cell.2007.11.019
22. McCauley KB, Hawkins F, Kotton DN. Derivation of epithelial-only airway organoids from human pluripotent stem cells. *Curr Protoc Stem Cell Biol*. 2018;45(1):e51. https://doi.org/10.1002/cpsc.51
23. Dobrindt K, Hoagland DA, Seah C, et al. Common genetic variation in humans impacts in vitro susceptibility to SARS-CoV-2 infection. *Stem Cell Rep*. 2021;16(3):505-518. https://doi.org/10.1016/j.stemcr.2021.02.010
24. Horowitz JC, Martinez FJ, Thannickal VJ. Mesenchymal cell fate and phenotypes in the pathogenesis of emphysema. *Copd*. 2009;6(3):201-210. https://doi.org/10.1080/15412550902905953
25. Hogan BL, Barkauskas CE, Chapman HA, et al. Repair and regeneration of the respiratory system: complexity, plasticity, and mechanisms of lung stem cell function. *Cell Stem Cell*. 2014;15(2):123-138. https://doi.org/10.1016/j.stem.2014.07.012
26. Al Alam D, El Agha E, Sakurai R, et al. Evidence for the involvement of fibroblast growth factor 10 in lipofibroblast formation during embryonic lung development. *Development (Cambridge, England)*. 2015;142(23):4139-4150. https://doi.org/10.1242/dev.109173
27. Juul NH, Stockman CA, Desai TJ. Niche cells and signals that regulate lung alveolar stem cells in vivo. *Cold Spring Harbor Perspect Biol*. 2020: 1;12(12):a035717. https://doi.org/10.1101/cshperspect.a035717
28. Muus C, Luecken MD, Eraslan G, et al. Integrated analyses of single-cell atlases reveal age, gender, and smoking status associations with cell type-specific expression of mediators of SARS-CoV-2 viral entry and highlights inflammatory programs in putative target cells. *Nat Med*. 2021;27(3):546-559. https://doi.org/10.1038/s41591-020-01227-z.
29. Zhang H, Rostami MR, Leopold PL, et al. Expression of the SARS-CoV-2 ACE2 receptor in the human airway epithelium. *Am J Respir Crit Care Med*. 2020;202(2):219-229. https://doi.org/10.1164/rccm.202003-0541OC
30. Lippi G, Henry BM. Chronic obstructive pulmonary disease is associated with severe coronavirus disease 2019 (COVID-19). *Respir Med*. 2020;167:105941. https://doi.org/10.1016/j.rmed.2020.105941
31. Cyranoski D. Profile of a killer: the complex biology powering the coronavirus pandemic. *Nature*. 2020;581(7806):22-26. https://doi.org/10.1038/d41586-020-01315-7
32. Zepp JA, Morrisey EE. Cellular crosstalk in the development and regeneration of the respiratory system. *Nat Rev Mol Cell Biol*. 2019;20(9):551-566. https://doi.org/10.1038/s41580-019-0141-3
33. Basil MC, Katzen J, Engler AE, et al. The cellular and physiological basis for lung repair and regeneration: past, present, and future. *Cell Stem Cell*. 2020;26(4):482-502. https://doi.org/10.1016/j.stem.2020.03.009
34. Zacharias WJ, Frank DB, Zepp JA, et al. Regeneration of the lung alveolus by an evolutionarily conserved epithelial progenitor. *Nature*. 2018;555(7695):251-255. https://doi.org/10.1038/nature25786
35. Hogan BLM. *The Alveolar Stem Cell Niche of the Mammalian Lung*. Singapore: Springer Singapore; 2020:7-12.
36. Miller AJ, Dye BR, Ferrer-Torres D, et al. Generation of lung organoids from human pluripotent stem cells in vitro. *Nat Protocols*. 2019;14(2):518-540. https://doi.org/10.1038/s41596-018-0104-8
37. Sacco O, Silvestri M, Sabatini F, et al. Epithelial cells and fibroblasts: structural repair and remodelling in the airways. *Paediatr Respir Rev*. 2004;5(Suppl A):S35-S40. https://doi.org/10.1016/s1526-0542(04)90008-5
38. Vij N, Chandramani-Shivalingappa P, Van Westphal C, Hole R, Bodas M. Cigarette smoke-induced autophagy impairment accelerates lung aging, COPD-emphysema exacerbations and pathogenesis. *Am J Physiol Cell Physiol*. 2018;314(1):C73-C87. https://doi.org/10.1152/ajpcell.00110.2016
39. Wendisch D, Dietrich O, Mari T, et al. SARS-CoV-2 infection triggers profibrotic macrophage responses and lung fibrosis. *Cell*. 2021;184(26):6243-6261.e27. https://doi.org/10.1016/j.cell.2021.11.033
40. Juul NH, Stockman CA, Desai TJ. Niche cells and signals that regulate lung alveolar stem cells in vivo. *Cold Spring Harbor Perspect Biol*. 2020;12(5):a040303. https://doi.org/10.1101/cshperspect.a040303
41. Antony VB, Thannickal VJ. Cellular senescence in chronic obstructive pulmonary disease: multifaceted and multifunctional. *Am J Respir Cell Mol Biol*. 2018;59(2):135-136. https://doi.org/10.1165/rcmb.2018-0061ED
42. Okuda R, Aoshiba K, Matsushima H, et al. Cellular senescence and senescence-associated secretory phenotype: comparison of idiopathic pulmonary fibrosis, connective tissue disease-associated interstitial lung disease, and chronic obstructive pulmonary disease. *J Thorac Dis*. 2019;11(3):857-864. https://doi.org/10.21037/jtd.2019.02.11
43. King PT. Inflammation in chronic obstructive pulmonary disease and its role in cardiovascular disease and lung cancer. *Clin Transl Med*. 2015;4(1):68. https://doi.org/10.1186/s40169-015-0068-z
44. Woldhuis RR, Heijink IH, van den Berge M, et al. COPD-derived fibroblasts secrete higher levels of senescence-associated secretory phenotype proteins. *Thorax*. 2021;76(5):508-511. https://doi.org/10.1136/thoraxjnl-2020-215114
45. Barnes PJ. The cytokine network in chronic obstructive pulmonary disease. *Am J Respir Cell Mol Biol*. 2009;41(6):631-638. https://doi.org/10.1165/rcmb.2009-0220TR
46. Kearley J, Silver JS, Sanden C, et al. Cigarette smoke silences innate lymphoid cell function and facilitates an exacerbated type I interleukin-33-dependent response to infection. *Immunity*. 2015;42(3):566-579. https://doi.org/10.1016/j.immuni.2015.02.011
47. Redhu NS, Gounni AS. Function and mechanisms of TSLP/TSLPR complex in asthma and COPD. *Clin Exp Allergy*. 2012;42(7):994-1005. https://doi.org/10.1111/j.1365-2222.2011.03919.x

48. Traves SL, Culpitt SV, Russell RE, Barnes PJ, Donnelly LE. Increased levels of the chemokines GROalpha and MCP-1 in sputum samples from patients with COPD. *Thorax*. 2002;57(7):590-595. https://doi.org/10.1136/thorax.57.7.590
49. Bhat TA, Panzica L, Kalathil SG, Thanavala Y. Immune dysfunction in patients with chronic obstructive pulmonary disease. *Ann Am Thorac Soc*. 2015;12(Suppl 2):S169-S175. https://doi.org/10.1513/AnnalsATS.201503-126AW
50. Morissette MC, Parent J, Milot J. Alveolar epithelial and endothelial cell apoptosis in emphysema: what we know and what we need to know. *Int J Chron Obstruct Pulmon Dis*. 2009;4:19-31.
51. Suwara MI, Green NJ, Borthwick LA, et al. IL-1α released from damaged epithelial cells is sufficient and essential to trigger inflammatory responses in human lung fibroblasts. *Mucosal Immunol*. 2014 7;7(3):684-693. https://doi.org/10.1038/mi.2013.87
52. Silva BSA, Lira FS, Ramos D, et al. Severity of COPD and its relationship with IL-10. *Cytokine*. 2018;106:95-100.
53. Houssaini A, Breau M, Kebe K, et al. mTOR pathway activation drives lung cell senescence and emphysema. *JCI Insight*. 2018;3(3):e93203. https://doi.org/10.1172/jci.insight.93203
54. Brusselle GG, Joos GF, Bracke KR. New insights into the immunology of chronic obstructive pulmonary disease. *Lancet (London, England)* 2011;378(9795):1015-1026. https://doi.org/10.1016/S0140-6736(11)60988-4
55. Attaway AA, Zein J, Hatipoglu US. SARS-CoV-2 infection in the COPD population is associated with increased healthcare utilization: an analysis of Cleveland clinic's COVID-19 registry. *EClinicalMedicine*. 2020;26:100515. https://doi.org/10.1016/j.eclinm.2020.100515
56. Chan LLY, Anderson DE, Cheng HS, et al. The establishment of COPD organoids to study host-pathogen interaction reveals enhanced viral fitness of SARS-CoV-2 in bronchi. *Nat Commun*. 2022;13(1):7635. https://doi.org/10.1038/s41467-022-35253-x
57. Letko M, Marzi A, Munster V. Functional assessment of cell entry and receptor usage for SARS-CoV-2 and other lineage B betacoronaviruses. *Nat Microbiol*. 2020;5(4):562-569. https://doi.org/10.1038/s41564-020-0688-y
58. Hoffmann M, Kleine-Weber H, Schroeder S, et al. SARS-CoV-2 cell entry depends on ACE2 and TMPRSS2 and is blocked by a clinically proven protease inhibitor. *Cell*. 2020;181(2):271-280.e8. https://doi.org/10.1016/j.cell.2020.02.052
59. Ziegler CGK, Allon SJ, Nyquist SK, et al. SARS-CoV-2 receptor ACE2 is an interferon-stimulated gene in human airway epithelial cells and is detected in specific cell subsets across tissues. *Cell*. 2020;181(5):1016-1035.e19. https://doi.org/10.1016/j.cell.2020.04.035
60. Mulay A, Konda B, Garcia G, et al. SARS-CoV-2 infection of primary human lung epithelium for COVID-19 modeling and drug discovery. *Cell Rep*. 2021; 35(5):109055. https://doi.org/10.1016/j.celrep.2021.109055.
61. Huang J, Hume AJ, Abo KM, et al. SARS-CoV-2 infection of pluripotent stem cell-derived human lung alveolar type 2 cells elicits a rapid epithelial-intrinsic inflammatory response. *Cell Stem Cell*. 2020;27(6):962-973.e7. https://doi.org/10.1016/j.stem.2020.09.013
62. Sanchez EL, Lagunoff M. Viral activation of cellular metabolism. *Virology*. 2015;479-480:609-618. https://doi.org/10.1016/j.virol.2015.02.038
63. Katze MG, He Y, Gale M. Viruses and interferon: a fight for supremacy. *Nat Rev Immunol*. 2002;2(9):675-687. https://doi.org/10.1038/nri888
64. Mulay A, Konda B, Garcia G Jr, et al. SARS-CoV-2 infection of primary human lung epithelium for COVID-19 modeling and drug discovery. *Cell Rep*. 2021;35(5):109055. https://doi.org/10.1016/j.celrep.2021.109055
65. Ueki IF, Min-Oo G, Kalinowski A, et al. Respiratory virus-induced EGFR activation suppresses IRF1-dependent interferon λ and antiviral defense in airway epithelium. *J Exp Med*. 2013;210(10):1929-1936. https://doi.org/10.1084/jem.20121401
66. Liu T, Zhang L, Joo D, Sun S-C. NF-κB signaling in inflammation. *Signal Transduct Target Ther*. 2017;2(1):e17023.
67. Venkataraman T, Coleman CM, Frieman MB. Overactive epidermal growth factor receptor signaling leads to increased fibrosis after severe acute respiratory syndrome coronavirus infection. *J Virol*. 2017;91(12):e00182-e00117. https://doi.org/10.1128/JVI.00182-17
68. Melchjorsen J, Sørensen LN, Paludan SR. Expression and function of chemokines during viral infections: from molecular mechanisms to in vivo function. *J Leukoc Biol*. 2003;74(3):331-343. https://doi.org/10.1189/jlb.1102577
69. Ishikawa E, Nakazawa M, Yoshinari M, Minami M. Role of tumor necrosis factor-related apoptosis-inducing ligand in immune response to influenza virus infection in mice. *J Virol*. 2005;79(12):7658-7663. https://doi.org/10.1128/JVI.79.12.7658-7663.2005
70. Pham I, Uchida T, Planes C, et al. Hypoxia upregulates VEGF expression in alveolar epithelial cells in vitro and in vivo. *Am J Physiol Lung Cell Mol Physiol*. 2002;283(5):L1133-L1142. https://doi.org/10.1152/ajplung.00464.2001
71. Blanco-Melo D, Nilsson-Payant BE, Liu W-C, et al. Imbalanced host response to SARS-CoV-2 drives development of COVID-19. *Cell*. 2020;181(5):1036-1045.e9. https://doi.org/10.1016/j.cell.2020.04.026
72. Spagnolo P, Balestro E, Aliberti S, et al. Pulmonary fibrosis secondary to COVID-19: a call to arms? *Lancet Respir Med*. 2020;8(8):750-752. https://doi.org/10.1016/S2213-2600(20)30222-8
73. Jacobs M, Van Eeckhoutte HP, Wijnant SRA, et al. Increased expression of ACE2, the SARS-CoV-2 entry receptor, in alveolar and bronchial epithelium of smokers and COPD subjects. *Eur Respir J*. 2020;56(2):2002378. https://doi.org/10.1183/13993003.02378-2020
74. Verhelst J, Parthoens E, Schepens B, Fiers W, Saelens X. Interferon-inducible protein Mx1 inhibits influenza virus by interfering with functional viral ribonucleoprotein complex assembly. *J Virol*. 2012;86(24):13445-13455. https://doi.org/10.1128/JVI.01682-12
75. Higham A, Mathioudakis A, Vestbo J, Singh D. COVID-19 and COPD: a narrative review of the basic science and clinical outcomes. *Eur Respir Rev*. 2020;29(158):200199. https://doi.org/10.1183/16000617.0199-2020
76. Chung KF, Adcock IM. Multifaceted mechanisms in COPD: inflammation, immunity, and tissue repair and destruction. *Eur Respir J*. 2008;31(6):1334-1356. https://doi.org/10.1183/09031936.00018908
77. Choi Y, Bowman JW, Jung JU. Autophagy during viral infection—a double-edged sword. *Nat Rev Microbiol*. 2018;16(6):341-354. https://doi.org/10.1038/s41579-018-0003-6
78. Olloquequi J. COVID-19 Susceptibility in chronic obstructive pulmonary disease. *Eur J Clin Invest*. 2020;50(10):e13382. https://doi.org/10.1111/eci.13382
79. Zost SJ, Gilchuk P, Case JB, et al. Potently neutralizing and protective human antibodies against SARS-CoV-2. *Nature*. 2020;584(7821):443-449. https://doi.org/10.1038/s41586-020-2548-6
80. Yang J, Zuo WL, Fukui T, et al. Smoking-dependent distal-to-proximal repatterning of the adult human small airway epithelium. *Am J Respir Crit Care Med*. 2017;196(3):340-352. https://doi.org/10.1164/rccm.201608-1672OC
81. McDonough JE, Yuan R, Suzuki M, et al. Small-airway obstruction and emphysema in chronic obstructive pulmonary disease. *N Engl J Med*. 2011;365(17):1567-1575. https://doi.org/10.1056/NEJMoa1106955
82. Ghaedi M, Calle EA, Mendez JJ, et al. Human iPS cell-derived alveolar epithelium repopulates lung extracellular matrix. *J Clin Invest*. 2013;123(11):4950-4962. https://doi.org/10.1172/JCI68793
83. Baarsma HA, Skronska-Wasek W, Mutze K, et al. Noncanonical WNT-5A signaling impairs endogenous lung repair in COPD. *J Exp Med*. 2017;214(1):143-163.

84. Zepp JA, Zacharias WJ, Frank DB, et al. Distinct mesenchymal lineages and niches promote epithelial self-renewal and myofibrogenesis in the lung. *Cell*. 2017;170(6):1134-1148.e10. https://doi.org/10.1016/j.cell.2017.07.034
85. Pinto BGG, Oliveira AER, Singh Y, et al. ACE2 expression is increased in the lungs of patients with comorbidities associated with severe COVID-19. *J Infect Dis* 2020;222(4):556-563. https://doi.org/10.1093/infdis/jiaa332
86. Hansen J, Baum A, Pascal KE, , et al. Studies in humanized mice and convalescent humans yield a SARS-CoV-2 antibody cocktail. *Sci* 2020;369(6506):1010-1014. https://doi.org/10.1126/science.abd0827
87. Chen P, Nirula A, Heller B, et al; BLAZE-1 Investigators. SARS-CoV-2 neutralizing antibody LY-CoV555 in outpatients with Covid-19. *N Engl J Med*. 2021;384(3):229-237. https://doi.org/10.1056/NEJMoa2029849
88. Hawkins F, Kramer P, Jacob A, et al. Prospective isolation of NKX2-1-expressing human lung progenitors derived from pluripotent stem cells. *J Clin Invest*. 2017;127(6):2277-2294. https://doi.org/10.1172/JCI89950
89. Wei J, Alfajaro MM, DeWeirdt PC, et al. Genome-wide CRISPR screens reveal host factors critical for SARS-CoV-2 infection. *Cell*. 2021;184(1):76-91.e13. https://doi.org/10.1016/j.cell.2020.10.028
90. Paila U, Chapman BA, Kirchner R, et al. GEMINI: an integrative exploration of genetic variation and genome annotations. *PLoS Comput Biol*. 2013;9(7):e1003153. https://doi.org/10.1371/journal.pcbi.1003153.
91. Ewels P, Magnusson M, Lundin S, Käller M. MultiQC: summarize analysis results for multiple tools and samples in a single report. *Bioinformatics*. 2016;32(19):3047-3048. https://doi.org/10.1093/bioinformatics/btw354
92. Korotkevich G, Sukhov V, Budin N, et al. Fast gene set enrichment analysis. 2021:060012. https://doi.org/10.1101/060012Bio
93. Wu T, Hu E, Xu S, et al. clusterProfiler 40: A universal enrichment tool for interpreting omics data. *Innovation* 2021;2(3):100141.
94. Yu G, Wang LG, Han Y, He QY. clusterProfiler: an R package for comparing biological themes among gene clusters. *OMICS J Integr Biol*. 2012;16(5):284-287. https://doi.org/10.1089/omi.2011.0118
95. Kanehisa M, Goto S, Furumichi M, Tanabe M, Hirakawa M. KEGG for representation and analysis of molecular networks involving diseases and drugs. *Nucleic Acids Res*. 2010;38 (Database issue):D355-D360. https://doi.org/10.1093/nar/gkp896
96. Jassal B, Matthews L, Viteri G, et al. The reactome pathway knowledgebase. *Nucleic Acids Res*. 2020;48(D1):D498-D503. https://doi.org/10.1093/nar/gkz1031
97. Ashburner M, Ball CA, Blake JA, et al. Gene ontology: tool for the unification of biology The Gene Ontology Consortium. *Nat Genet*. 2000;25(1):25-29. https://doi.org/10.1038/75556
98. Liberzon A, Birger C, Thorvaldsdóttir H, et al. The Molecular Signatures Database (MSigDB) hallmark gene set collection. *Cell Syst*. 2015;1(6):417-425. https://doi.org/10.1016/j.cels.2015.12.004
99. Gu Z, Eils R, Schlesner M. Complex heatmaps reveal patterns and correlations in multidimensional genomic data. *Bioinformatics*. 2016;32(18):2847-2849. https://doi.org/10.1093/bioinformatics/btw313